Ca2+ Dependant Synaptic Modification

by

Dongsung Huh

Submitted to the Department of Physics
in partial fulfillment of the Requirements
for the Degree of

BACHELOR OF SCIENCE

at the

Massachusetts Institute of Technology

June 4th, 2004

Signature of Author .....
Department of Physics/ Department of Brain and Cognitive Sciences
May 7th, 2004

Certified by .....
Guosong Liu
Associate Professor of Department of Brain and Cognitive Sciences
Thesis Supervisor

Accepted by .....
David E. Pritchard
Senior Thesis Coordinator, Department of Physics

Ca^{2+} Dependant Synaptic Modification

Dongsung Huh

MIT Department of Physics & Brain and Cognitive Sciences

May 17, 2004

Abstract

It has been assumed that Ca^{2+} influx of different duration and amplitude would generate different level of potentiation. The conventional protocols of generating LTP have been 1. tetanic stimulation of presynaptic cell, 2. theta burst stimulation of presynaptic cell, and 3. correlated stimulation of pre- and postsynaptic cells. However, the effects of different Ca^{2+} influx can not be precisely dissected with the conventional protocols for the following defects: 1. the protocols do not discriminate between pre- and postsynaptic side plasticity, 2. the protocols observe synaptic plasticity between two cells which involve multiple synapses with heterogenous properties, 3. precise control and measurement of the amount of Ca^{2+} influx are not possible in the protocols. In the present experiment, we perfused glutamate directly on to a single postsynaptic site, depolarized the postsynaptic intracellular potential to a controlled voltage for a controlled duration of time, thus controlling the opening of postsynaptic NMDA receptors and Ca^{2+} influx. By using this method, we found 1. that modification of synaptic strength has a bell-shaped dependency to the amount of Ca^{2+} influx, 2. that weak Ca^{2+} current through desensitized NMDA receptors sustained for a long period of time (160 ms) generates LTD, 3. evidence that phosphorylation of AMPAR leads to insertion of AMPAR.

1 Introduction

The human brain, a huge neural network, consists of roughly 10 billion neurons and 50 to 100 trillions synaptic connections between the neurons. These connections are the cellular substrate of higher cognitive functions such as learning, memory, and consciousness. As a brain matures, the synaptic connections also mature, becoming more refined, functional and numerous, as the brain develops cognitive skills.

The higher cognitive functions and any other information that are stored in brain are encoded in terms of strength of synaptic connections. Therefore, modification of synaptic strength - the process called synaptic plasticity - during the maturation process is believed to be the fundamental basis of learning and memory. In behavioral experiments, it was found that when animals learn information from experiences, their synaptic connections of certain brain areas show structural and functional changes, and more over when they were treated with drugs that cease further modification of synapses, the animals could not store new memories.

Therefore, the modification of synaptic strength depends on external events, or more specifically, the spatio-temporal patterns of neural activity which reflect the external events. A neural network controls its synaptic properties in such a way that the network ends up encoding certain amount of information of the experience it has gone through. In 1949, Donald Hebb postulated that such a control of synaptic modification is in fact embraced in the properties of individual synapses.

Hebb's conjecture is the following: if input from neuron A often contributes to the neuronal activity firing of neuron B, then the synapse from A to B will be strengthened.[1] Hebb suggested that such synaptic modification could produce neuronal assemblies that reflect the relationships experienced during training. For example, consider applying this rule to neurons that fire together during training due to an association between a stimulus and a response. These neurons would develop strong interconnections, and subsequent activation of some of them by the stimulus could produce the synaptic drive needed to activate the remaining neurons and generate the associated response. Hebb's original suggestion concerned increases in synaptic strength, but it has been generalized to include decreases in strength arising from the repeated failure of neuron A to be involved in the activation of neuron B. The general form of the Hebb rule state that synapses change in proportion to the correlation or covariance of the activities of the pre-and postsynaptic neurons.

Hebb's activity-dependent-synaptic-plasticity was confirmed in cultured neurons

and slices of mammalian brain which is generally termed Long-Term-Potentiation (LTP). LTP is a stable and enduring increase in the magnitude of the synaptic response of neurons after appropriate electrical stimuli have been applied to the presynaptic cell and postsynaptic cell. LTP has been found in all excitatory pathways in the hippocampus, as well as in several other regions in the brain, and there is growing evidence that it underlies at least certain forms of memory.[4][5] The conventional stimuli protocol for artificially generating LTP is tetanus - stimulating the presynaptic cell with high frequency, high amplitude current pulses, which generate large synaptic current enough to activate the postsynaptic cells correspondingly.[6][7] Bi and Poo (1998) invented another stimulation protocol and clearly showed that LTP is dependent on spike-timings of a pair of neurons (pre- and postsynaptic neurons).[?] When presynaptic cell was constantly stimulated to fire spikes 2$\sim$20 ms prior to postsynaptic cell spike activity (positive temporal correlation), their synaptic response increased in size. When the neurons were stimulated in reverse order (negative temporal correlation), their synaptic response decreased (Long-Term-Depression, LTD).

It is known that Ca^{2+} current through NMDA receptor channels on the postsynaptic site triggers modification of the synapse: When NMDA channel blocker, D-AP-5 or 7-Chlorokynurenic acid, was injected in the extracellular solution, LTP and LTD was blocked, and the animal could not learn new memories.[8][9] Current view of the field is that high-amplitude, short duration ($\sim$ tens of milliseconds) pulses of Ca^{2+} currents into the post- side of a synapse increase the synaptic strength, while low-amplitude, long duration (over hundreds of milliseconds) pulses of Ca^{2+} ion currents decrease strength. However, the effects of different Ca^{2+} influx can not be precisely dissected with conventional LTP/LTD generation protocols due to the following limitations: 1. the protocols do not discriminate between pre- and postsynaptic side plasticity, 2. the protocols observe synaptic plasticity between two cells which involve multiple synapses with heterogenous properties, 3. precise control and measurement of the amount of Ca^{2+} influx are not possible in the protocols.

In the present study, we introduce a new technique which involves stimulation and response of the postsynaptic site of a single synapse. The technique also allows us to control and estimate the amplitude and duration of Ca^{2+} current through NMDA receptors of the postsynaptic site. With this new powerful tool, we have partially characterized the dependence of synaptic modification on the amount and duration of Ca^{2+} influx during activities of neurons.

For the readers without prior knowledge of neuroscience, I will review the structure

and functions of neurons and synapses before further proceeding into the details of the research.

2 Introduction to Neurons and Synapses

2.1 Neurons

Neurons are specialized for generating electrical signals in response to several types of (mostly chemical) stimulus inputs, and transmitting them to other cells. Important morphological structures are the dendrites that receive inputs from other neurons and the axon that carries the neuronal output to other cells. The dendritic tree allows a neuron to receive inputs from many other neurons through synaptic connections.

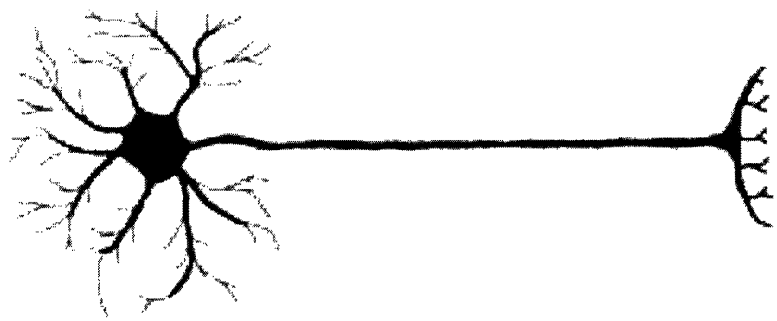

Figure 1: Schematic picture of neuron with its three defined regions: the cell body and the dendrites, and the axon.

2.1.1 Membrane Voltage, Equilibrium Potential

The electrical signal of relevance to the nervous system is the difference in electrical potential between the interior of a neuron and the surrounding extracellular medium. The intracellular voltage fluctuates as ionic current flows in and out through membrane-spanning ion channels. Ion channels control the flow of ions across the cell membrane by opening and closing in response to voltage changes and to both internal and external signals. Ions involved in the electrical activities of neurons are mostly sodium (Na^+), potassium (K^+), calcium (Ca^{2+}), and chloride (Cl^-).

Flow of ions through open ion channels is controlled by voltage difference and concentration gradient across the membrane. Consider, or example, a positively charged

(q) ion and a negative membrane potential (V). In this case, ions are free to flow into the cell and therefore the inward ionic current is simply proportional to the concentration of ions outside of the cell ([outside]). However, ions inside the cell can flow out of the cell only if they have sufficient thermal energy to overcome the energy barrier $|qV|$. According to the Boltzmann distribution of energies, the probability of an ion to have thermal energy larger than $|qV|$ is $\exp\left(\frac{-|qV|}{kT}\right)$. Therefore, the outward ionic current is proportional to [inside]$*\exp\left(\frac{qV}{kT}\right)$. At a particular potential, called equilibrium potential V_{E}, the net flow of ions will be 0 when the inward and outward flows are equal.

$$[\text{outside}] = [\text{inside}] * \exp\left(\frac{qV_E}{kT}\right),$$

Therefore, the equilibrium potential is

$$V_E = \frac{kT}{q} \ln\left(\frac{[\text{outside}]}{[\text{inside}]}\right) \qquad \text{(Nernst Equation)} \tag{1}$$

Therefore, equilibrium potential for each species of ions is determined by the ion's charge and intracellular and extracellular distribution. The equilibrium potential for a K^+ conducting channel, E_K, typically falls in the range between -70 and -90 mV. The Na^+ equilibrium potential, E_{Na}, is 50 mV or higher, and E_{Ca}, for Ca^{2+} channels, is higher still, around 150 mV. Cl^- equilibrium potentials are typically around -60 to -65 mV, near the resting potential of many neurons. In all cases, the surrounding extracellular medium is the ground.

Under resting condition, conductance of K^+ channels of neurons are 20$\sim$100 times larger than other types of ion channels and keeps the intracellular voltage of a neuron near its equilibrium potential E_K ($\simeq -70$ mV), and the cell is said to be polarized. Any of mechanical, electrical or chemical perturbations on a neuron would would trigger opening certain types of ion channels and move the membrane potential up or down toward the ion channel's equilibrium potential. When a cell's membrane potential is more negative than its resting potential, the cell is said to be hyper-polarized. When a cell's membrane potential is less negative or even positive values the cell is said to be depolarized.

2.1.2 Action Potential

When a neuron receives enough depolarizing current to raise the membrane potential above a threshold level ($\simeq$ -20 mV), a positive feed back process induces a sharp depolarization (up to 20$\sim$ 30 mV) followed by slight hyper-polarization called an action

potential, or shortly, a spike. At threshold voltage, voltage-gated Na^+ channels start to open, which shoots the membrane potential up toward the equilibrium potential of Na^+, 50 mV, then opening of voltage-gated K^+ channels brings down toward K^+ ion equilibrium potential, which is -90 mV. Duration of an action potential is about 1 ms.

A neuron fires action potentials at the cell body (soma) and axon, but not at dendrites. Action potential travels down along the axon as a chain reaction: An action potential at a patch of membrane depolarizes the next patch inducing a second action potential, and so on. An action potential is an effective form of electrical signal that can propagate over large distance without noise or loss of signal.

When an action potential fires at the cell body, the fluctuation of electric field also travels toward dendritic sites passively through intracellular cytoplasm. This passive process - referred to as back propagating dendritic spike - is believed to play a crucial role in correlated activity dependent synaptic plasticity.

2.2 Synapse

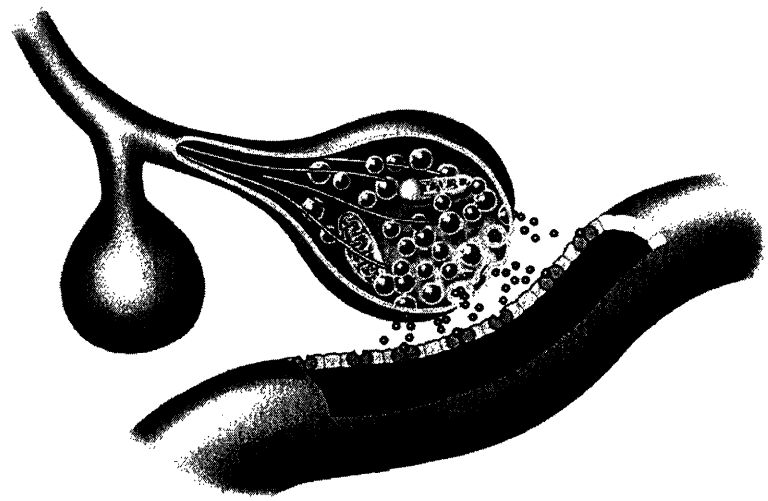

Figure 2: A schematic picture of synapse showing the presynaptic axon terminal, postsynaptic dendritic area, release of neurotransmitters and postsynaptic receptors. (Excerpted from http://www.scientific-art.com/)

A synapse is a narrow junction where two neurons communicate chemically. When a action potential arrives at a synapse of signal-sending, or the presynaptic neuron,

vesicles filled with neurotransmitter are released. The neurotransmitter then binds to receptors at the signal-receiving or postsynaptic side of the synapse, causing ion-conducting channels to open. Depending on the nature of the ion flow, the synapses an have either an excitatory, depolarizing, or an inhibitory typically hyperpolarizing, effect on the postsynaptic neuron. The strength of a synaptic connection is determined by the size of excitatory or inhibitory current through the postsynaptic site induced by a single action potential of the presynaptic cell.

Two important neurotransmitters in central nervous system are glutamate acid and GABA. At excitatory synapses, binding of glutamate to glutamatergic receptors on postsynaptic cell opens ion channels which conducts Na^+, K^+, and Ca^{2+} and depolarize the cell. At inhibitory synapses, GABA binds to GABAergic receptors which opens Cl^- conducting ion channels and hyperpolarize the postsynaptic cell.

AMPA receptor (AMPAR) and NMDA receptor (NMDAR) are two most important glutamatergic receptor ion channels . AMPAR and NMDAR can be selectively blocked with different drugs so that their properties can be separately studied. The response of AMPAR and NMDAR to release of neurotransmitters are quite different.

2.2.1 Conductance of AMPA Receptors

AMPAR channels work in a simple mechanism. An AMPAR channel is in the open state when glutamate is bounded to it and in the closed state when glutamate is unbounded. Transition between the two states is probabilistic and is described by the following equation.

$$\frac{dP_{\text{glu}}}{dt} = \alpha_{\text{glu}}(1 - P_{\text{glu}}) - \beta_{\text{glu}} P_{\text{glu}} \tag{2}$$

Here, P_{glu} is the probability of a channel being in the open state, α_{glu} is the opening rate of the closed channels, which is proportional to concentration of glutamate near the receptor, and β_{glu} is the closing rate of the open channels, which is essentially constant.

When an action potential in the presynaptic cell releases glutamate, the glutamate concentration increases extremely rapidly, remains high for approximately 1 ms, and then falls rapidly to 0. We can simplify the fluctuation of glutamate concentration as a narrow square pulse of duration T ($\simeq$ 1 ms) at the moment of presynaptic action potential and 0 everywhere else. Integrate Equation 2 under this assumption, we

obtain

$$P_{\text{glu}}(t) = 1 - e^{-\alpha_{\text{glu}} t} \quad \text{for} \quad 0 \le t \le T \tag{3}$$

$$P_{\text{glu}}(t) = P_{\max} e^{-\beta_{\text{glu}}(t-T)} \quad \text{for} \quad t \ge T \quad (\text{ where } \quad P_{\max} = P_{\text{glu}}(T)\ ) \tag{4}$$

for fast synapses like AMPA receptors

$$P_{\text{glu}}(t) \simeq P_{\max} \exp(-t/\tau_{\text{glu}}) \tag{5}$$

$$\tau_{\text{glu}} = 1/\beta_{\text{glu}} \tag{6}$$

The AMPAR conductance is proportional to $P_{\text{glu}}(t)$.

$$g_{\text{AMPA}} \propto P_{\text{glu}}(t) \tag{7}$$

Conductance of a channel differs for different ions. AMPAR channels are most conductive to Na^+ and k^+.

2.2.2 Conductance of NMDA Receptors

The mechanism of NMDAR is more complex, because it involves magnesium block. NMDAR has a Mg^{2+} binding site on its ion conducting pathway which is blocked when Mg^{2+} is bound on it. Therefore, NMDAR opens only when both two conditions are met: binding of glutamate and unbinding of Mg^{2+}. Binding of Mg^{2+} on NMDAR is voltage dependent which can be described in terms of statistical physics. The energy difference between the Mg^{2+} bound state and unbound state is where E_0 is the binding energy and δV is the partial voltage difference that Mg^{2+} feels. Transition rate from the NMDAR–Mg^{2+} bound state to the unbound state is proportional to the probability of a particle to have thermal energy larger than ΔE, $\int_{\Delta E}^{\infty} \exp\left(-\frac{E}{kT}\right) dE = \exp\left(-\frac{\Delta E}{kT}\right)$. On the other hand, the binding rate of Mg^{2+} to an unblocked NMDAR is simply proportional to the concentration of Mg^{2+} ions ($[Mg^{2+}]$) in the vicinity of the receptor. The probability of an unblocked NMDAR state is then described by the following equation.

$$\frac{dP_{\text{Mg}}}{dt} = -\alpha_{\text{Mg}}[Mg^{2+}]P_{\text{Mg}} + \beta'_{\text{Mg}} \exp\left(\frac{\delta q V}{kT}\right)(1 - P_{\text{Mg}}) \tag{8}$$

(where $\beta'_{\text{Mg}} = \beta_{\text{Mg}} \exp(-E_0/kT)$, β_{Mg}: unbinding rate constant). At equilibrium condition ($\frac{dP_{\text{Mg}}}{dt} = 0$), Equation 8 gives the unblocked probability of NMDAR as

$$P_{\text{Mg}}(V) = \left(1 + [Mg^{2+}]\frac{\alpha_{\text{Mg}}}{\beta'_{\text{Mg}}} \exp(-\delta q V/kT)\right)^{-1}, \tag{9}$$

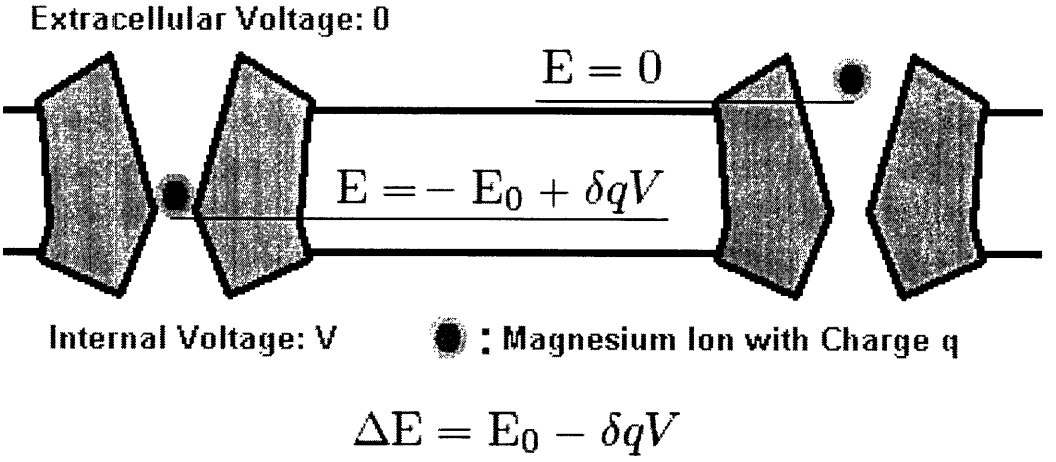

Figure 3: Schematic diagram of NMDAR structure.

In 1990, Jahr and Stevens matched this result to empirical data and concluded that

$$P_{\mathrm{Mg}}(V) = \left(1 + \frac{[\mathrm{Mg}^{2+}]}{3.57\mathrm{mM}} \exp(-V/16.13\mathrm{mV})\right)^{-1} \tag{10}$$

NMDA receptors are open only when both glutamate is bound to it and Mg^{2+} blockade is removed. Therefore, the conductance of NMDAR is proportional to

$$g_{\mathrm{NMDA}}(t, V) \propto P_{\mathrm{glu}}(t) P_{\mathrm{Mg}}(V) \tag{11}$$

where $P_{\mathrm{glu}}(t)$ is expressed as Equation 3 and Equation 4, but it has smaller binding and unbinding rates compare to AMPAR. Conductivity of a channel differs for different ion types. NMDAR channels are conductive to Na^+, K^+ and Ca^{2+}.

Therefore, NMDA receptors open only for correlated activity of pre- and postsynaptic cells: presynaptic glutamate release and the postsynaptic membrane voltage elevation. For this reason, NMDA receptors are also referred to as "the coincidence detector".

2.2.3 Current through Membrane Channels: Goldman-Hodgkin-Katz Equation

Equation 7 and Equation 11 tell us the conductance of AMPA and NMDA to which their mediated currents are proportional. However, calculation of the actual amount of current involves more consideration of movements of ions in fluid. Ions in fluid move

around by diffusion and drift. Under electric field, ions drift with the velocity at which the electric force and viscosity friction cancel each other. $\vec{v}_{\text{drift}} = \vec{F}_E \mathcal{B} = q\mathcal{B}\vec{\nabla}V$, where $\mathcal{B}$ is the friction constant. Therefore, the drift flux is

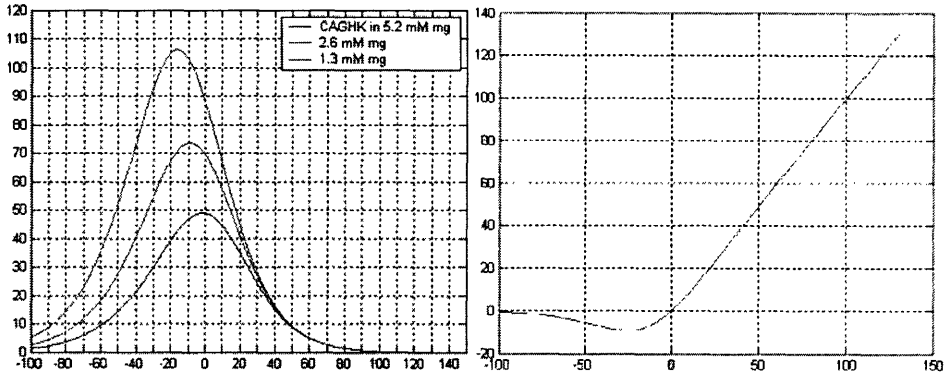

Figure 4: **Left**: Plot of NMDAR mediated Ca^{2+} current under 2.6 mM Ca^{2+} and [5.2, 2.6, and 1.3 mM] Mg^{2+} extracellular concentrations according to GHK and Woodhull equations. During induction protocol, cells were under extracellular solution with 1.3 mM Mg^{2+} and 2.6 mM Ca^{2+}. **Right**: Plot of the total amount of NMDAR mediated ionic current under 1.3 mM Mg^{2+} and 2.6 mM Ca^{2+} extracellular condition according to Equation 17. The current axis (y-axis) in both plots are in an arbitrary unit.

$$\vec{J}_{\text{drift}} = \rho\vec{v}_{\text{drift}} = -\rho q\mathcal{B}\vec{\nabla}V, \tag{12}$$

where ρ is the number density of the ions. When the solution is not homogeneous, ions diffuse from higher concentration region to lower concentration region. Fick discovered that the diffusion flux is proportional to concentration gradient.

$$\vec{J}_{\text{diffuse}} = -\mathcal{D}\vec{\nabla}\rho, \tag{13}$$

where the diffusion constant $\mathcal{D}$ has thermodynamic interpretation as

$$\mathcal{D} = \mathcal{B}kT \qquad (\text{ Einstein's relationship. See Appendix A.3})$$

Therefore the total flux of ions is

$$\vec{J} = \vec{J}_{\text{drift}} + \vec{J}_{\text{diffuse}} = -\mathcal{B}kT\left(\vec{\nabla}\rho + \beta\rho q\vec{\nabla}V\right) \quad (\text{where } \beta = 1/kT) \tag{14}$$

Using the integration factor $e^{\beta qV(x)}$, the above equation can be rewritten as

$$\vec{J}e^{\beta qV(x)} = -\mathcal{B}kT\vec{\nabla}\left(\rho(x)e^{\beta qV(x)}\right). \tag{15}$$

Goldman-Hodgkin-Katz assumed 1 dimensional channel model and constant field in membrane, that is

$$V(x) = Vx/d, \quad (0 \leq x \leq d),$$

where x is the position in the 1 dimensional channel pathway. In this case, Equation 15 can be easily integrated and rearranged.

$$J = \frac{\mathcal{B}qV}{d} \frac{\rho_{\text{out}} - \rho_{\text{in}} e^{\beta qV}}{e^{\beta qV} - 1} \tag{16}$$

where setting $J = 0$ gives the Nernst Equation (Eq. 1). Ions are assumed not to interfere with other types of ions, and the total current through a channel is the summation of all ion flux.

$$I_{\text{total}} = g_{\text{Na}} J_{\text{Na}} + g_{\text{K}} J_{\text{K}} + g_{\text{Ca}} J_{\text{Ca}}, \tag{17}$$

where conductances are given as functions of voltage and time (Equation 7, Equation 11). Plots in Figure 4 show NMDAR mediated Ca^{2+} current in different Mg^{2+} concentration and the total current in 1.3mM of extracellular Mg^{2+} concentration as predicted by Equation 17.

2.3 Synaptic Plasticity

The process by which the strength of a synapse changes over time is called synaptic plasticity. Synaptic plasticity involves both pre- and postsynaptic changes. Presynaptically, the probability of releasing neurotransmitter vesicles and the amount of neurotransmitters contained in a single vesicle can change.[10] Postsynaptic changes involve insertion[11][12][13])/exertion ([14][15][16][17][18])of receptors and activation/inactivation of receptors through phosphorylation/dephosphorylation.[19][20][21][22]

Most of postsynaptic change is due to change of AMPAR response, while NMDAR current size remains constant. Instead, NMDAR is involved in control mechanism of AMPAR modification. NMDAR mediated Ca^{2+} current is known to trigger a cascade of plasticity reactions, one of which phosphorylates AMPARs and increase their ionic conductance, and another triggers insertion of AMPAR from non-synaptic areas into the synapse.[8][9] Correlated activities of pre- and postsynaptic neurons introduces a large Ca^{2+} current through NMDAR, which is believed to be the underlying mechanism of Hebb's activity-dependent-synaptic-plasticity postulate.

In the present experiment, we Several experimental evidences suggest that different magnitudes and patterns of postsynaptic [Ca^{2+}] influx can selectively induce LTP

or LTD. For example, high-amplitude, short duration (tens of milliseconds) pulses of Ca^{2+} currents into the post- side of a synapse induce LTP, while low-amplitude, long duration (over hundreds of milliseconds) pulses of Ca^{2+} ion currents induce LTD. However, the exact effect of Ca^{2+} current of different properties has not yet been experimentally confirmed.

3 Experiment

To directly measure the effect of NMDAR mediated Ca^{2+} current through single post-synaptic site, we used two powerful techniques. To gain control of electric potential of the postsynaptic cell and measure the current flowing in and out from the cell, we used whole-cell-perforated-patch-clamping method. For local application of glutamate on to a single synaptic site, we used the iontophoresis technique.

3.1 Experimental Tools

3.1.1 Perforated Whole Cell Patch Recording

Perforated whole cell patch clamping is a powerful technique for controlling and/or recording intracellular membrane potentials and currents. A hollow glass pipette electrode filled with conducting electrolytes makes a tight connection with a neuron membrane. After the patch electrode seals (up to GΩ of electrical resistance), the perforation chemical (amphotericin B) starts to introduce pores onto the membrane beneath the electrode tip, providing electrical contact or resistance of 10 20 MΩ, called access resistance, with the interior of the cell. A series of 10 ms step depolarization pulses from -70 to -60 mV were applied to assay access resistance according to the circuit model in Figure 5. Access resistance of less than 30 mega-Ω were required to swiftly change a neuron's intracellular voltage.

For our experiment, we used a protocol called voltage clamp: We controlled the intracellular potential to the desired voltage by injecting current to maintain the voltage. The injection of current was recorded, which is equivalent to the current passing through the entire cell membrane.

3.1.2 High-resolution Iontophoresis

The number and properties of functional postsynaptic receptors can be assessed directly by their responses to local application of transmitter. LTP could also be gen-

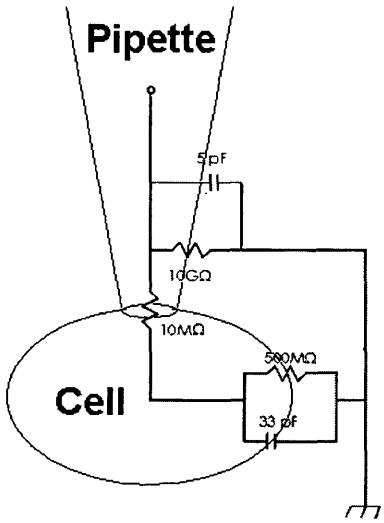

Figure 5: A schematic diagram of whole cell patch clamp method. A diagram of an equivalent circuit is overlapped.

erated by the same method. For elaborate generation and measurement of post-synaptic modification, we used iontophoresis technique to directly stimulate a single post-synaptic site in the physiological time scale (0.5 ms). Our iontophoresis electrode is a quartz pipette filled with an glutamate acid solution (150 mM) with a tip opening smaller than the synaptic size (0.1 microns).

Such a narrow tip is required both to prevent leakage during non-stimulation, and to restrict the area of glutamate diffusion within a single synapse. However, the narrow-tip, high resistance electrode resulted in a long RC time constant τ of 200 ms (R$\simeq$100 MΩ, C$\simeq$0.2 nF). The low-filter property of the system becomes an obstacle for ejection of single pulses of 0.5 ms. To help minimize this problem, we decreased R by pulling electrodes with a short shank, as a long, thin shank increases electrode resistance. We lowered the extracellular solution level as much as possible since the submerged portion of the electrode contributes to capacitance. To compensate for the remaining RC filtering, we used a positive-feedback capacitance compensation in the stimulation current.

To properly adjust the capacitance compensation, we applied a -10 nA square-wave pulse at 20 Hz to the iontophoresis electrode after filling it and immersing the tip in the bath. We monitored the tip voltage on an oscilloscope while adjusting the compensation so that the voltage also described a square wave. With the proper

capacitance compensation setting, the iontophoresis electrode could inject a pulse of glutamate of 64 nA amplitude and 0.5 ms duration. [23]

A Patch electrodes was mounted on MP-285 micro-manipulator (Sutter Instrument) and the iontophoresis electrode was mounted on MPC-100 micro-manipulator (Sutter Instrument) to be controlled in sub-micrometer precision.

3.2 Experimental Procedure

The protocol for our experiment was the following: 1. We patch-clamped a neuron, voltage-clamped it at -70 mV in an extracellular bath solution which was designed to block NMDA receptors - we call it the baseline solution (See B.4 section for the composition of baseline solution and induction solution). To locate synaptic sites we used a fluorescent presynaptic marker FM1-43 (See B.2) for the composition of FM1-43 solution). We brought the iontophoresis electrode to the 1μm vicinity to a single synaptic site and measured baseline synaptic current in response to local application of glutamate for 5 to 10 minutes (Baseline-recording of initial synaptic strength). 2. Then the bath solution was switched into the induction solution which enables NMDAR channels to open. We ran an induction protocol which induces a specific amount of Ca^{2+} influx through NMDAR channels (Induction of synaptic change). 3. We switched the bath solution back to the baseline solution and measured synaptic responses as in step 1 until the size of synaptic current stabilized (Post-modification measurement of synaptic strength).

For the analysis, the amplitude of synaptic response current of step 1 and step 3 were compared for the measurement of potentiation of the single postsynaptic site.

NMDAR blocker was used during step 1 and step 3 because the test pulses of glutamate (64 nA for 1 ms, for the measurement of synaptic current size) were so large that introduced a large AMPAR mediated current which locally depolarized the postsynaptic site. Without NMDAR blocker, some amount of Ca^{2+} would flow into the cell and cause potentiation of the postsynaptic site during baseline measurement - we call this effect "creeping" (See Figure 10). Therefore, NMDAR blocker was mixed in baseline solution to avoid creeping and measure the exact size of initial and final postsynaptic responses.

We tested several NMDAR blockers. The commonly used NMDAR blocker, D-AP-5, could not efficiently block NMDAR mediated current (Figure 7). It is because D-AP-5 is a competitive glutamate site blocker and becomes rivaled out to pulses of high concentration of glutamate. Creeping was observed during the measurement in

AP5 added baseline solution. Then, we tested a non-competitive glycine site blocker of NMDAR, 7-Chlorokynurenic acid (Glycine is another requirement for opening of NMDAR channels). Use of this drug completely blocked NMDAR mediated current and creeping effect (Figure 11), but it also decreased the AMPAR current drastically (see Figure 8 and Figure12). Our analysis involved only relative changes in AMPAR response size, therefore data obtained in this baseline solution was still usable. However, blocking of AMPAR might have an unknown effect in cells metabolism and is not desirable. Finally, we employed 5,7-Di-Chlorokynurenic acid - a variation of 7-Chlorokynurenic acid - for the baseline solution, in which NMDAR current was completely blocked and AMPAR current size was mostly unaffected (Figure 9).

3.3 Induction Protocol

During the induction phase (step 2), neurons were immersed in induction solution. Our LTP induction protocol involves local application of glutamate and depolarization of the postsynaptic neuron which opens NMDAR channels. There was 40ms gap between the glutamate pulse and postsynaptic depolarization due to the fact NMDAR takes 40ms to open with maximum probability. We controlled the depolarization voltage and duration of the depolarization. The amount of Ca^{2+} influx was estimated according to Figure 4. See the table below for the specifications of protocols.

To ensure that our iontophoresis technique does induce potentiation as classical methods do, we employed an additional protocol which applies 5 pulses of glutamate at 100Hz frequency for each stimulus similarly to the conventional presynaptic tetanic stimulation. However, the tetanic protocol does not allows us to estimate the amount of NMDAR mediated Ca^{2+} influx and thus was not analyzed further.

Protocol	Depolarization Voltage V(mV)	Depolarization Duration T(ms)	Stimulus Freq.(Hz)	Number of Cycles
Tetanus	N/A	N/A	0.2	40
−10.160.1	−10	160	1	100
−20.160.1	−20	160	1	100
−30.40.0.2	−30	40	0.2	50
−30.160.1	−30	160	1	100
+30.160.1	+30	160	1	100

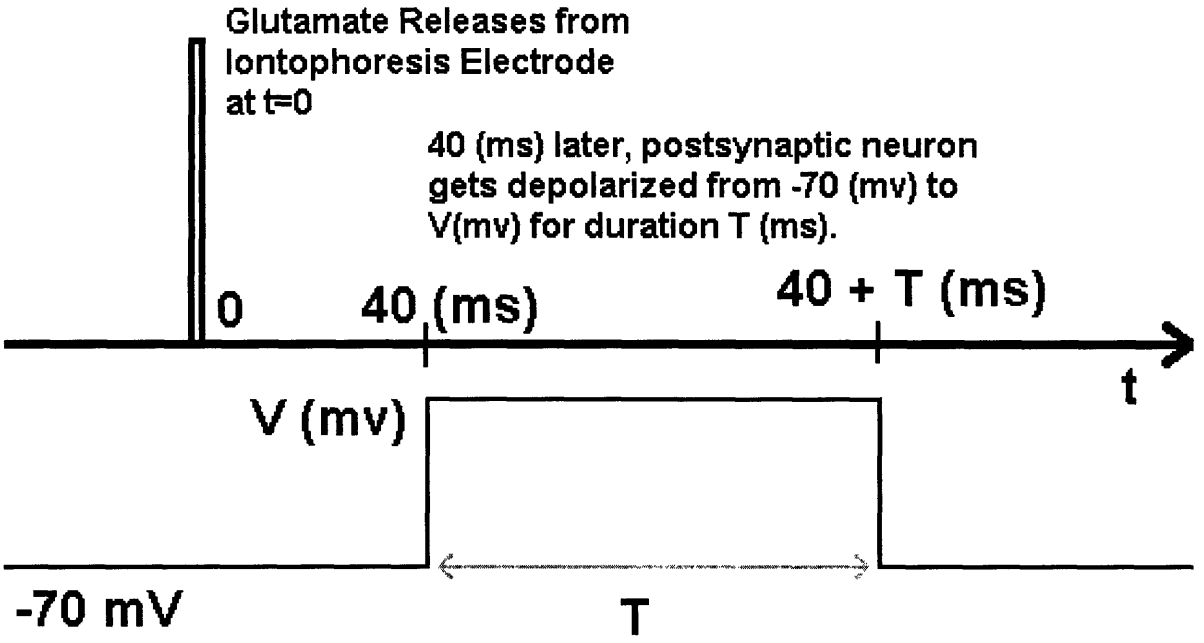

Figure 6: Explanatory figure for our induction protocol.

4 Results

Samples of recordings are shown in Figure 13∼16. Each protocol had different efficacy of generating potentiation. Figure 17 shows a summary of the potentiation results. On average, −10.160.1 generated $4.9 \pm 8.3\%$ increase, −30.160.1 generated $37 \pm 22\%$ increase, −30.40.0.2 generated $108 \pm 35\%$ increase, +30.160.1 generated $6.4 \pm 12\%$ increase, and tetanus evoked $43 \pm 9.1\%$ increase (Figure 17, upper). To understand the role of depolarization duration and stimulus frequency, I've grouped the results of x.160.40..1 protocols (160 ms, 1 Hz). The lower plot of Figure 17 clearly shows that 160ms, 1Hz protocols rarely induce potentiation, while 40 ms, 0.2Hz protocols produce massive potentiation, even more than classical potentiation due to tetanic stimulation.

Lack of potentiation in 160ms, 1Hz protocols was unexpected, because it would introduce maximum Ca^{2+} at each stimulation pulse and generate most potentiation. However, shorter duration and lower stimulation frequency protocols turned out to be more reliable for massive potentiation generation. We discovered that the 160ms 1 Hz protocols introduced a large initial Ca^{2+} influx that led the NMDA receptors into another state - desensitized. An NMDA receptor in the desensitized state does

not respond to binding of neurotransmitters until it recovers to functional states. 1 second interval between induction pulses of 160ms 1 Hz protocols was not sufficient for the receptors to recover from the desensitized state, and the NMDA mediated current was significantly decreased after several stimulation cycles (Figure 18). On the other hand, the NMDAR responses to 40ms 0.2 Hz induction protocol showed little change throughout all the stimulation cycles. (Figure 19) Therefore, during the 160ms 1 Hz induction protocols, except for the first few pulses, there was very little Ca^{2+} influx through NMDA receptors for a long period of time (160ms), which is currently believed to be the properties required for LTD induction stimulus protocol.

Further analysis of -30.40.0.2 showed an interesting relationship between the amount of functional NMDAR and change of synaptic strength (Figure 22). When the amount of functional NMDAR is small (less than 300 pA) there is a large positive correlation between the amount of NMDAR and potentiation amount, however when the amount of NMDAR exceeds a threshold (700 pA in this case), potentiation level drops, thus the overall shape of the curve becomes bell shaped. Since the amount of functional NMDAR is proportional to Ca^{2+} influx, we assert that this curve shows the relationship between Ca^{2+} influx and synaptic strength modification.

We also observed that the potentiation during induction protocol can predict the amount of post-induction potentiation. The ratio between the synaptic response in the beginning of induction and at the end of induction protocol (induction ratio) had a significant correlation with overall change of synaptic response (between step 1 and step 3). (Figure 24)

5 Discussion

The bell-shaped curve dependence of LTP on Ca^{2+} in Figure 22 is in close agreement with the previous result (Sadeghpour, unpublished Figure 23). This experiment was in fact designed to confirm the preliminary result of the bell-shaped dependence. The previous data involved creeping in baseline recordings and therefore the result was hard to be interpreted. Of course, the number of data-points in the Figure 22 is too small to conclude the assertion. Further research would eventually reveal the actual shape of the curve.

Generation of LTD due to small amplitude, long duration desensitized Ca^{2+} current partly confirms the wide-spread belief that small amount of sustained Ca^{2+}influx induces LTD. We are currently implementing a method to estimate the amount of

Ca^{2+} influx through desensitized NMDAR channels. Further research will involve more quantitative analysis of the effect of sustained, small-amplitude Ca^{2+} influx on LTD. It is very expected to find a vivid correlation between small Ca^{2+} current and LTD generation level.

The quick potentiation effect during induction protocol ($\sim$ 1 minute) is due to phosphorylation of AMPAR. The high positive correlation between induction ratio and overall synaptic strength change (Figure 24) strongly suggests that the short-term potentiation through phosphorylation undergoes transition into a long-term potentiation involving insertion of AMPAR. This result may explain the underlying mechanism of consolidation of short-term-potentiation into long-term-potentiation, and furthermore explain the consolidation process of short-term-memory into long-term-memory.

Synapses control the flow of current from one portion of the network to another, similar to the role of transistors in electronic circuits. This fundamental unit of computation of the brain also has an exquisite property that it modifies itself according to experience to encode information of the experience. Comprehension of how the fundamental learning process works in synaptic level will eventually lead to comprehension of learning algorithm of overall brain and the encoding and storage mechanism of information in brain.

Acknowledgements

I thank Safa Sadeghpour for his incessant supervision and advice. I am grateful to Guosong Liu for the lab equipment and for the wonderful experience with electrophysiology. I also thank Bing Li for continuous supply of cells.

List of Figures

References

[1] Hebb, D. O. *The Organization of Behavior* (Wiley, New York. 1949)

[2] Bliss, T. V. P. & Lomo, T. *J. Physiol., Lond.* **232,** 331-356 (1973).

[3] Bliss, T. V. P. & Gardner-Medwin, A. R. *J. Physiol., London.* **232,** 357-574 (1973).

[4] Morris, R. G. M., Davis, S. & Butcher, S. P. *Ohil. Trans. R. Soc.* **329,** 187-204 (1990).

[5] Doyere, V. & Laroche. S. *Hippocampus* **2**, 39-48 (1992)

[6] Larson, J., Wong. D. & Lynch. G. *Brain Res.* **368,** 347-350 (1986).

[7] Rose, G. M. & Dunwiddie, T. V. *Neurosci. Lett.***69,** 244-248 (1986)

[8] Collingridge, G. L., Kehl, S. J. & McLennan, H. *J. Pjysiol. Lond.* **334,** 33-46 (1983)

[9] Bashir, Z. I., Tam, B. & Collingridge, G. L. *Neurosci. Lett.* **80,** 111-114 (1987)

[10] Malgaroli, A. & Tsien, R. W. *Nature* **357,** 134-139 (1992)

[11] Shi, S.H., Hayashi, Y., Petralia, R.S., Zaman, S.H., Wenthold, R.J., Svoboda, K., and Malinow, R. *Science* **284,** 1811?1816 (1999).

[12] Hayashi, Y., Shi, S.H., Esteban, J.A., Piccini, A., Poncer, J.C., and Malinow, R. *Science* **287,** 2262?2267 (2000).

[13] Passafaro, M., Piech, V., and Sheng, M. *Nat. Neurosci.* **4,** 917?926 (2001).

[14] Carroll, R.C., Beattie, E.C., Xia, H., Lu scher, C., Altschuler, Y., Nicoll, R.A., Malenka, R.C., and von Zastrow, M. *Proc. Natl. Acad. Sci. USA* **96,** 14112?14117 (1999).

[15] Man, H.-Y., Lin, J.W., Ju, W.H., Ahmadian, G., Liu, L., Becker, L.E.,Sheng, M., and Wang, Y.T. *Neuron* **25,** 649?662 (2000).

[16] Ehlers, M.D. *Neuron* **28,** 511?525 (2000).

[17] Lin, J.W., Ju, W., Foster, K., Lee, S.H., Ahmadian, G., Wyszynski, M., Wang, Y.T., and Sheng, M. *Nat. Neurosci.* **3,** 1282?1290 (2000).

[18] Beattie, E.C., Carroll, R.C., Yu, X., Morishita, W., Yasuda, H., von Zastrow, M., and Malenka, R.C. *Nat. Neurosci.* **3,** 1291?1300 (2000).

[19] Reymann, K. G., Davies, S. N., Matthies, H., Kase, H. & Collingridge, G. L. *Eur. J. Neurosci.* **2,** 481-486 (1990).

[20] Gasic, G. P & Hollmann, M. *A. Rev. Physiol.* **54,** 507-536 (1992).

[21] Greengard, P., Jen, J., Nairn, A. C.& Stevens, C. F. *Science* **253,** 113-1138 (1991).

[22] Wang, L.-Y., Salter, M. W. & MacDonald, J. F. *Science* **253,** 1132-1135 (1991).

[23] Murnick, J.G., Dube, G.R., Krupa, B. & Liu G. *Journal of Neuroscience Methods* 116 65-75 (2002).

[24] Sadeghpour, S. (2003) Unpublished.

A Appendix

A.1 Brownian motion: Einstein-Smoluchowski theory

Let us now to study the Brownian motion from the point of view of diffusion. The variables under consideration are the number density of the Brownian particles in the fluid $\rho(\vec{r},t)$ and the current density of the particles $\vec{j}(\vec{r},t) = \rho(\vec{r},t)\vec{v}(\vec{r},t)$. The two fundamental laws are

$$\vec{j} = -\mathcal{D}\vec{\nabla}\rho \quad \text{the Fick's law, where } \mathcal{D} = \text{diffusion coefficient} \tag{18}$$

$$\vec{\nabla} \cdot \vec{j} + \frac{\partial \rho}{\partial t} = 0 \quad \text{Continuity Equation} \tag{19}$$

Substituting the Fick's law into the continuity equation, we obtain the diffusion equation

$$\nabla^2 \rho - \frac{1}{\mathcal{D}} \frac{\partial \rho}{\partial t} = 0 \tag{20}$$

Of the various possible solutions of this equation, the one relevant to the present problem is

$$\rho(\vec{r}, t) = \frac{\mathcal{N}}{(4\pi \mathcal{D} t)^{3/2}} \exp\left(-\frac{r^2}{4\mathcal{D}t}\right), \tag{21}$$

whose diffusion properties are

$$\langle \vec{r}(t) \rangle = 0 \tag{22}$$

$$\langle r^2(t) \rangle = \frac{1}{\mathcal{N}} \int_0^\infty r^2 \rho(\vec{r}, t)\ 4\pi r^2 dr = 6\mathcal{D}t. \tag{23}$$

for 3 dimensional case, $\mathcal{N}$=: total number of particles (Einstein-Smoluchowski)

In this approach, we are considering the motion of an ënsembleöf $\mathcal{N}$ Brownian particles placed under ëquivalentp̈hysical conditions. Accordingly, the averages of various physical quantities obtained here will be in the nature of ënsemble averages. Thus the ënsembleöf the Brownian particles, initially concentrated at the origin, d̈iffuses outäs time increases, the nature and the extent of its spread at any time being given by Equation 22 and Equation 23 respectively. The diffusion process gives us a fairly good picture of the statistical behavior of a single particle in ensemble.

A.2 Brownian motion: Langevin theory

Consider a free Brownian particle in a fluid, that is, a particle is assumed to feel only two types of forces: 1) the viscous drag $-\frac{\vec{v}}{\mathcal{B}}$ and 2) a r̈apidly and randomly fluctuatingf̈orce $\vec{F}(t)$, which averages out too zero over long intervals of time. Then the equation of motion of the particle will be

$$m\frac{d\vec{v}}{dt} = -\frac{\vec{v}}{\mathcal{B}} + \vec{F}(t), \quad (\langle \vec{F}(t) \rangle = 0) \quad \text{(Langevin)}, \tag{24}$$

and therefore,

$$\frac{d\vec{v}}{dt} = -\frac{\vec{v}}{\tau} + \vec{A}(t) \quad (\langle \vec{A}(t) \rangle = 0) \quad \text{where } \tau = m\mathcal{B} \tag{25}$$

We construct the scalar product of Equation 25 with the position $\vec{r}$ of the particle and take the ensemble average of the product. In doing so, we make use of the facts that,

$$\vec{r}\cdot\vec{v} = \frac{1}{2}\left(\frac{d}{dt}r^2\right),\ \vec{r}\cdot\frac{d}{dt}\vec{v} = \frac{d}{dt}(\vec{r}\cdot\vec{v}) - \vec{v}\cdot\frac{d}{dt}\vec{r} = \frac{1}{2}\frac{d}{dt}\left(\frac{d}{dt}r^2\right) - v^2, \text{ and } \langle\vec{r}\cdot\vec{A}\rangle = 0.$$

Therefore, we obtain,

$$\frac{d^2}{dt^2}\langle r^2\rangle + \frac{1}{\tau}\frac{d}{dt}\langle r^2\rangle = 2\langle v^2\rangle,$$

which can be rewritten by the use of integrating factor $e^{t/\tau}$ as,

$$\frac{d}{dt}\left(\frac{d}{dt}\langle r^2\rangle e^{t/\tau}\right) = 2\langle v^2\rangle e^{t/\tau} \tag{26}$$

At thermal equilibrium, the quantity $\langle v^2\rangle$ has its equipartition value $3kT/m$. The equation is then readily integrated with the result

$$\langle r^2\rangle = \frac{6kT\tau^2}{m}\left(\frac{t}{\tau} + e^{-t/\tau} - 1\right) \tag{27}$$

where the constants of integration have been so chosen that at time t=0 both $\langle r2\rangle$ and its first time-derivative vanish. We observe that, in macroscopic time scale $t \gg \tau$,

$$\langle r^2\rangle \simeq \frac{6kT\tau}{m}t = 6\mathcal{B}kTt \quad \text{when } t \gg \tau \tag{28}$$

A.3 Einstein's Relationship

By comparing the results of Langevin's approach and Einstein's approach of Brownian motion (Equation 23 and Equation 28) we obtain thermodynamic equation for the diffusion constant

$$\mathcal{D} = \mathcal{B}kT \tag{29}$$

which is often referred to as *Einstein's Relation.*

B Method

B.1 Cell Culture

Primary cultures of CA1-enriched hippocampal neurons were prepared from neonatal rats (P1). The age of the cultures used in this study range from 14 to 21 days in vitro (DIV). All experiments involving animals were approved by the Massachusetts Institute of Technology's Committee on Animal Care.

B.2 Fluorescent Imaging of Synapses

Functional presynaptic boutons were stained with 10 μM FM 1-43 (synaptogreen, Biotium). The composition of the FM1-43 staining solution was (in mM): KCl 90, NaCl 39, Glucose 30, HEPES 25, CaCl2 2, MgCl2 1, NBQX (6-nitro-7-sulphamoylbenzo[f]quinoxaline-2,3-dione) 0.005, D-AP-5 (DL-2-amino-5-phosphonovalerate) 0.1, and FM 1-43 0.01 (adjusted to pH 7.4 with NaOH).

B.3 Imaging

Imaging was taken using an Olympus (FV300) confocal laser inverted microscope. The 488 nm line of the argon laser was used for excitation, and the emitted light was filtered using a 510 nm long pass filter and detected by photomultiplier. A 40×1.15 NA water-immersion objective was used for imaging. For experiments, images were collected at a resolution of 1024×1024 with a pixel width of 0.11 μm. Confocal aperture was set to maximal. The gain of photomultiplier was adjusted to maximize the signal/noise ratio without causing the saturation by the strongest signals.

B.4 Electrophysiology

Whole cell perforated patch clamp recordings (Hamill et al., 1981; Horn and Marty, 1988; Rae et al., 1991) were made on cultured hippocampal pyramidal neurons. Perforated patch pipettes were front-filled with a solution containing (in mM): CsOH, 127; D-gluconic acid, 127; CsCl, 4; HEPES, 10; NaCl, 8; EGTA, 0.4; pH was adjusted to 7.2 with CsOH, and then back-filled with the same solution containing 150-220 ng/ml amphotericin B (Sigma, St. Louis, MO). We used two different extracellular solutions for the measurement (Baseline Solution) and for the induction protocols (Induction Solution). Baseline solution contained (in mM): NaCl, 145; KCl, 3; glucose, 15; HEPES, 10; MgCl2, 5.2; CaCl2, 1.3; 0.05 picrotoxin (Sigma); and for the induction phase extracellular solution contained (in mM): NaCl, 145; KCl, 3; glucose, 15; HEPES, 10; MgCl2, 1.3; CaCl2, 2.6; 0.005 glycine (Sigma), 0.05 picrotoxin (Sigma) and NMDA blocker (See 3.2 section); For both solutions pH was adjusted to 7.4 with NaOH. The extracellular bath solution was constantly perfused with fresh recording medium at slow rate through out recording, and at higher rate when switching the induction and baseline solutions. All experiments were performed at room temperature. Synaptic responses were recorded using a MultiClamp 700A amplifier (Axon

Instruments, Foster City, CA), digitized at 10 kHz with 1.2 kHz filtering.

Electrophysiological data was analyzed by a custom script written for Matlab (MathWorks, Natick, MA) by Safa Sadeghpour.

C Figures

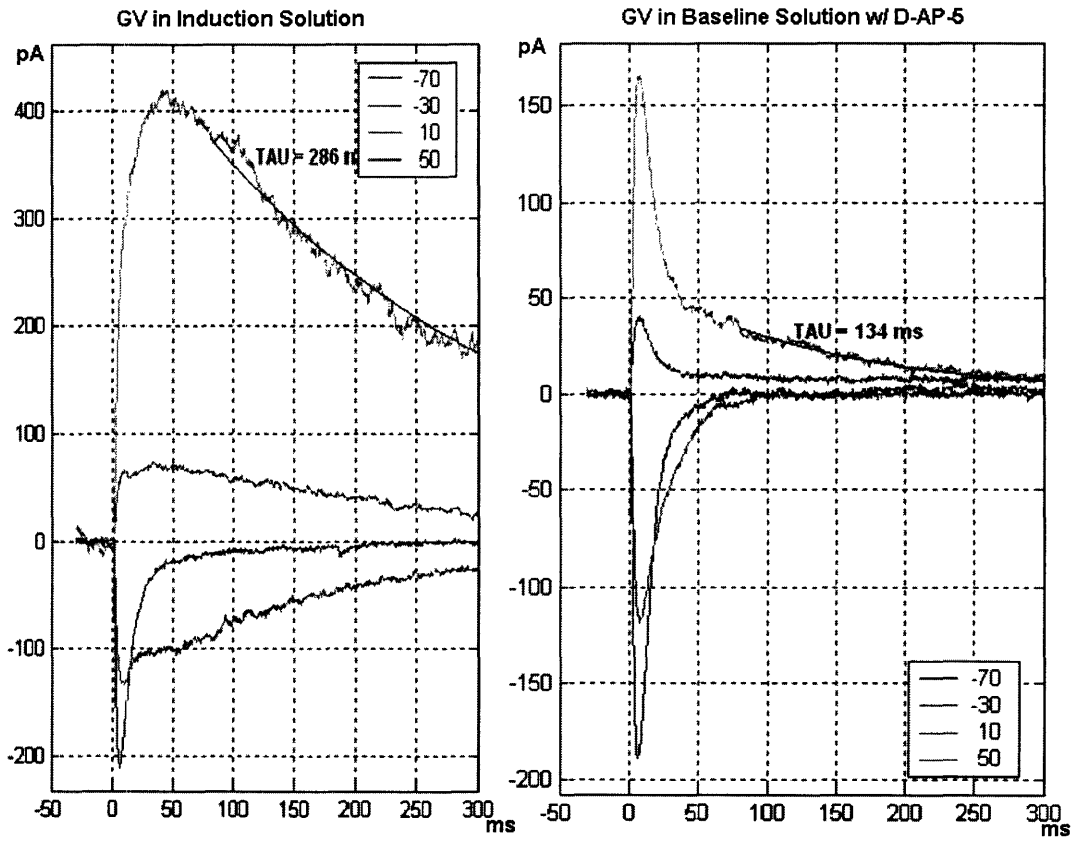

Figure 7: Recording of response of a synapse at different clamped voltage (-70, -30, 10, 50 mV) when immersed in induction-solution (left) and in baseline-solution with D-AP-5 (right). We fitted the curves to the GHK equation (Equation 17) and the conductance equations of AMPAR and NMDAR (Equation 7, Equation 11) to estimate the amount of active AMPA and NMDA receptors. The amount of receptors are expressed in terms of their peak response amplitude. The number of active NMDA receptors were reduced from 393 pA to 37 pA, and AMPA receptors from 196 pA to 147 pA at the presence of D-AP-5.

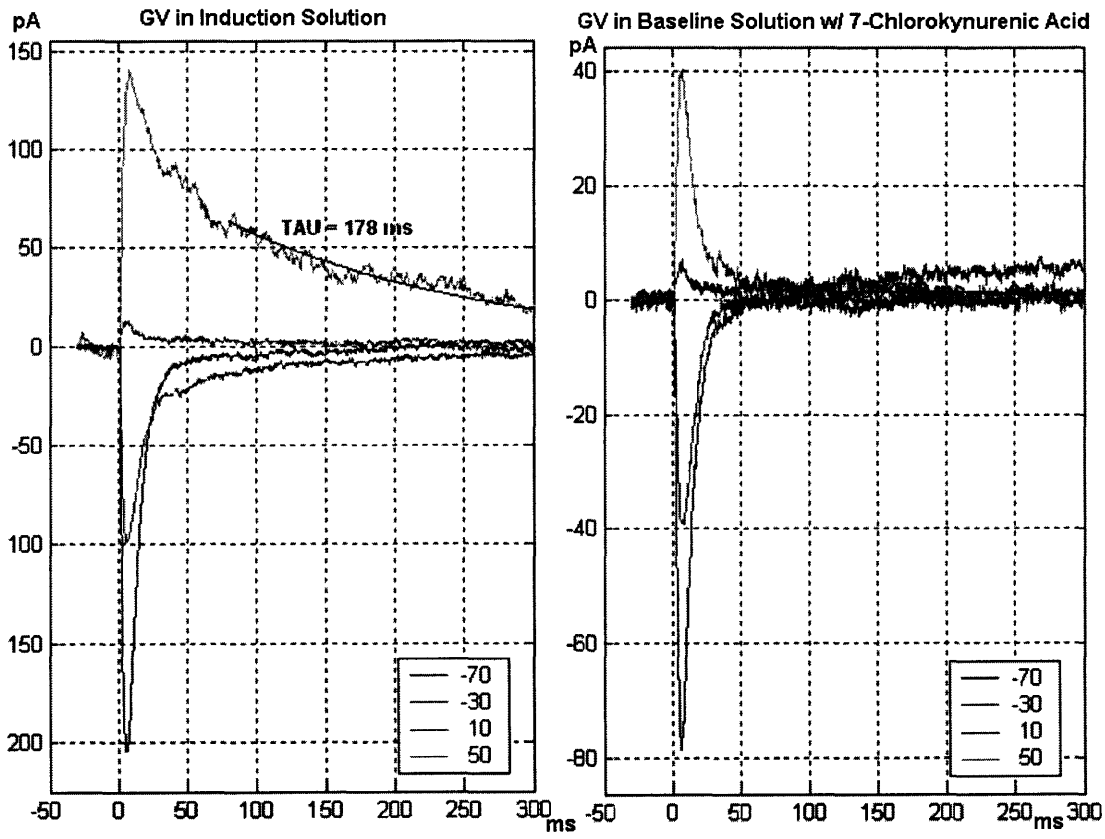

Figure 8: Change of synaptic response when immersed in induction-solution(left) and in baseline-solution with 7-Chlorokynurenic Acid (right). The number of active NMDA receptors were reduced from 81 pA to 3 pA, and AMPA receptors from 117 pA to 35 pA.

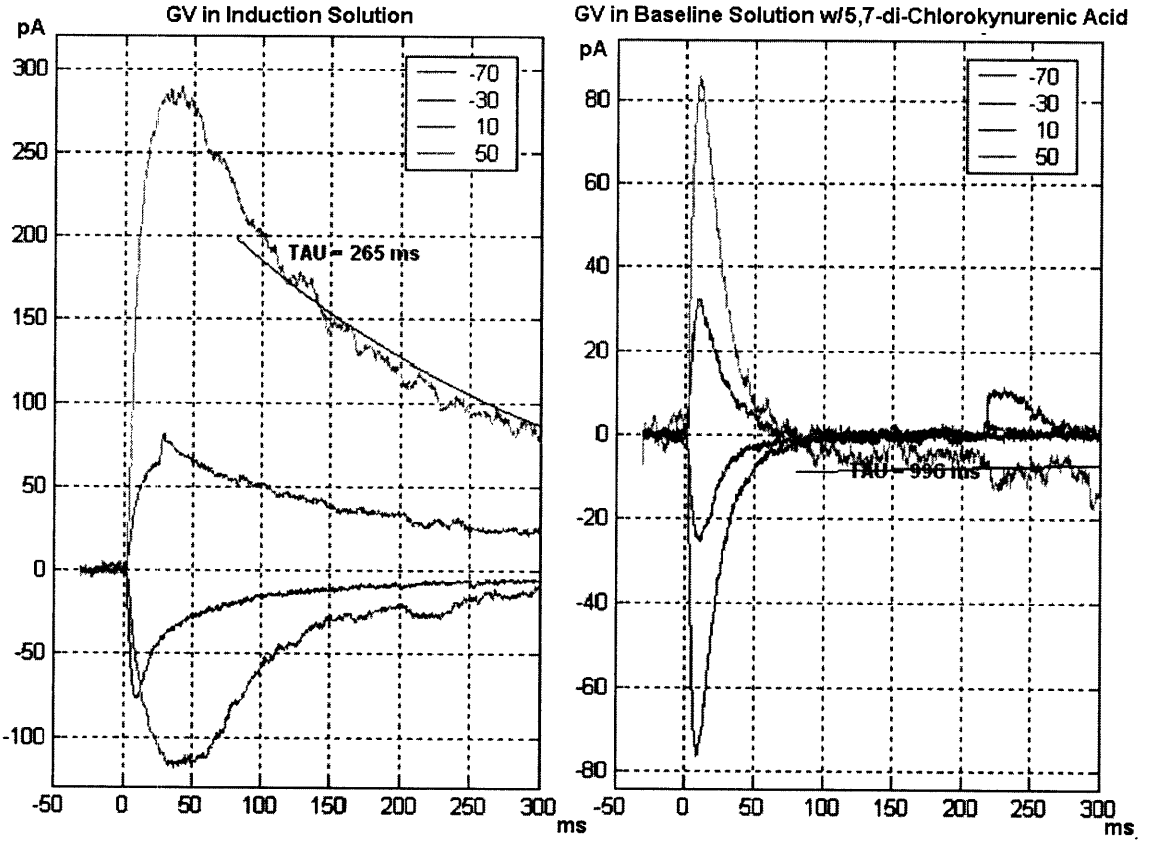

Figure 9: Change of synaptic response when immersed in induction-solution(left) and in baseline-solution with 5,7-Di-Chlorokynurenic Acid (right). The number of active NMDA receptors were reduced from 238 pA to 2 pA, and AMPA receptors from 69 pA to 55 pA.

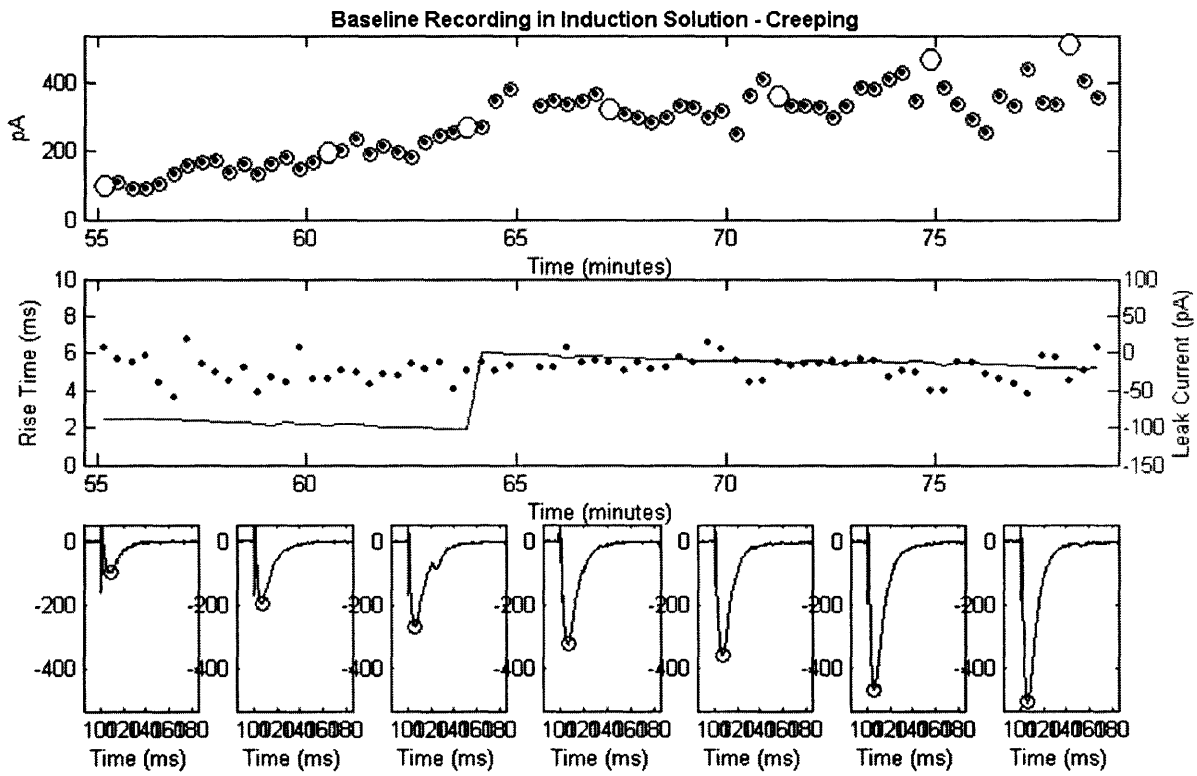

Figure 10: Baseline-recording in induction solution (no NMDA blocker, w/ Glycine). The uppermost figure is the plot of size of synaptic response current at each measurement time. Each event of measurement introduce NMDAR mediated Ca^{2+} influx and increase the next measurement size of synaptic response. The middle figure shows the initial rise time of the response. Rise time is an increasing function of distance between iontophoresis electrode and synapse. Therefore, we endeavored to keep the rise time constant in small range (4 8 ms), by bringing iontophoresis electrode as near to a synapse as possible. The lowermost figures are traces of sample synaptic response recordings. Each trace corresponds to an empty circle in the uppermost figure.

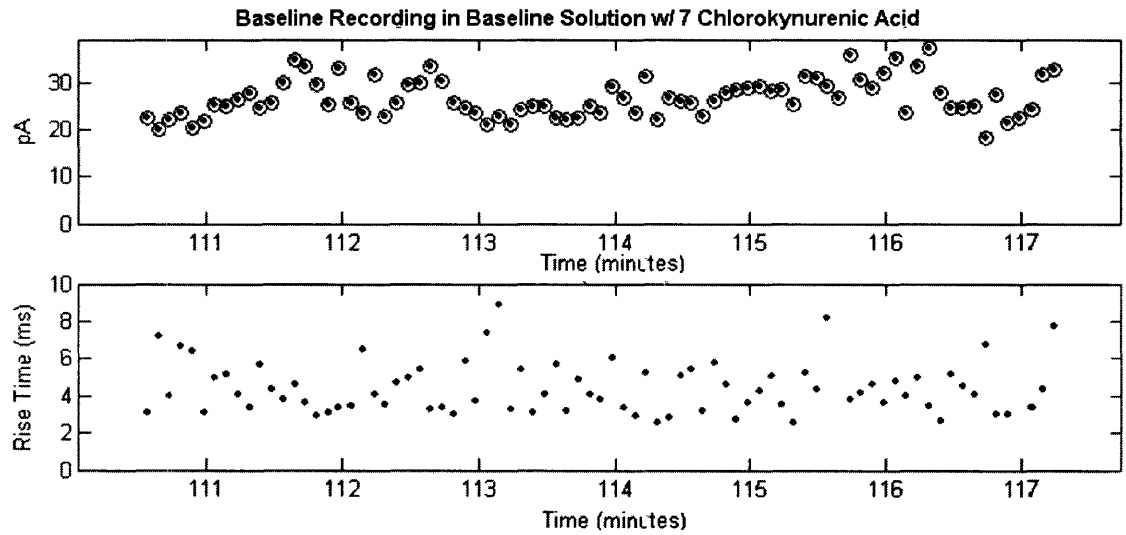

Figure 11: No creeping effect in baseline-solution with 7-Chlorokynurenic acid.

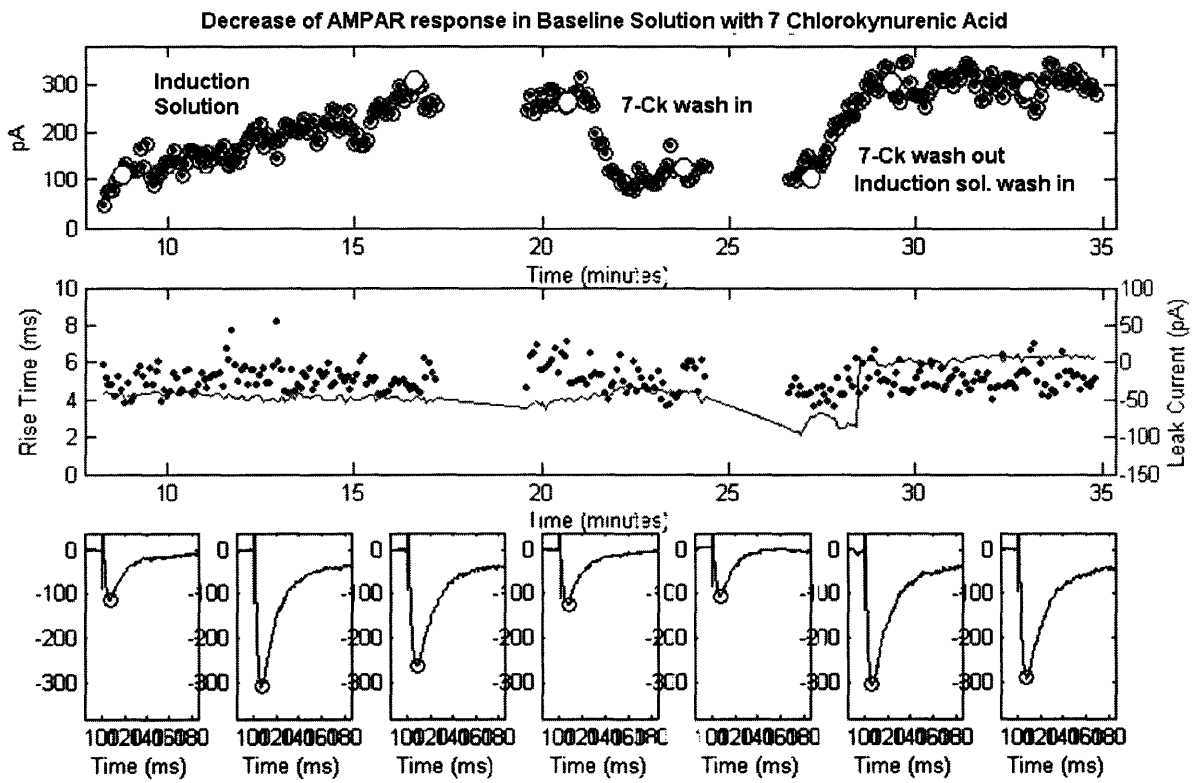

Figure 12: Effect of 7-Chlorokynurenic acid on AMPAR response size. 7-CK blocks AMPAR as well as NMDAR.

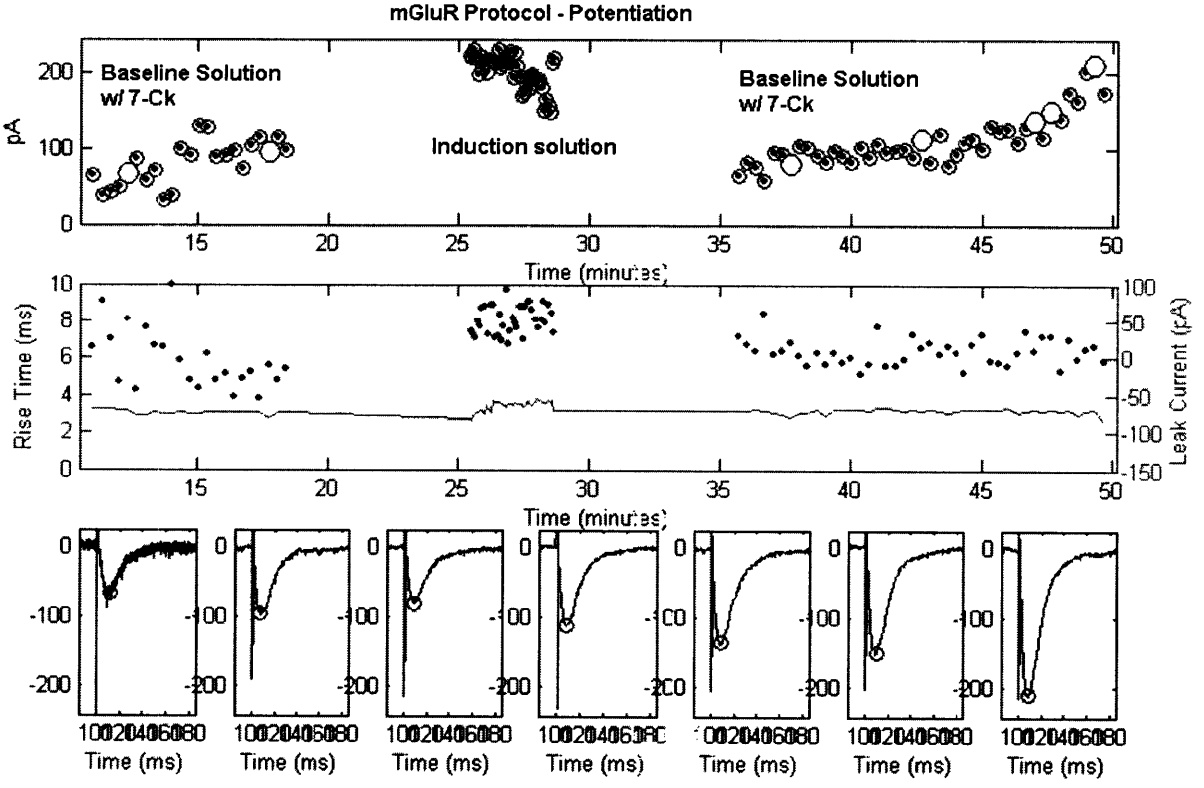

Figure 13: Tetanic stimulation generates potentiation.

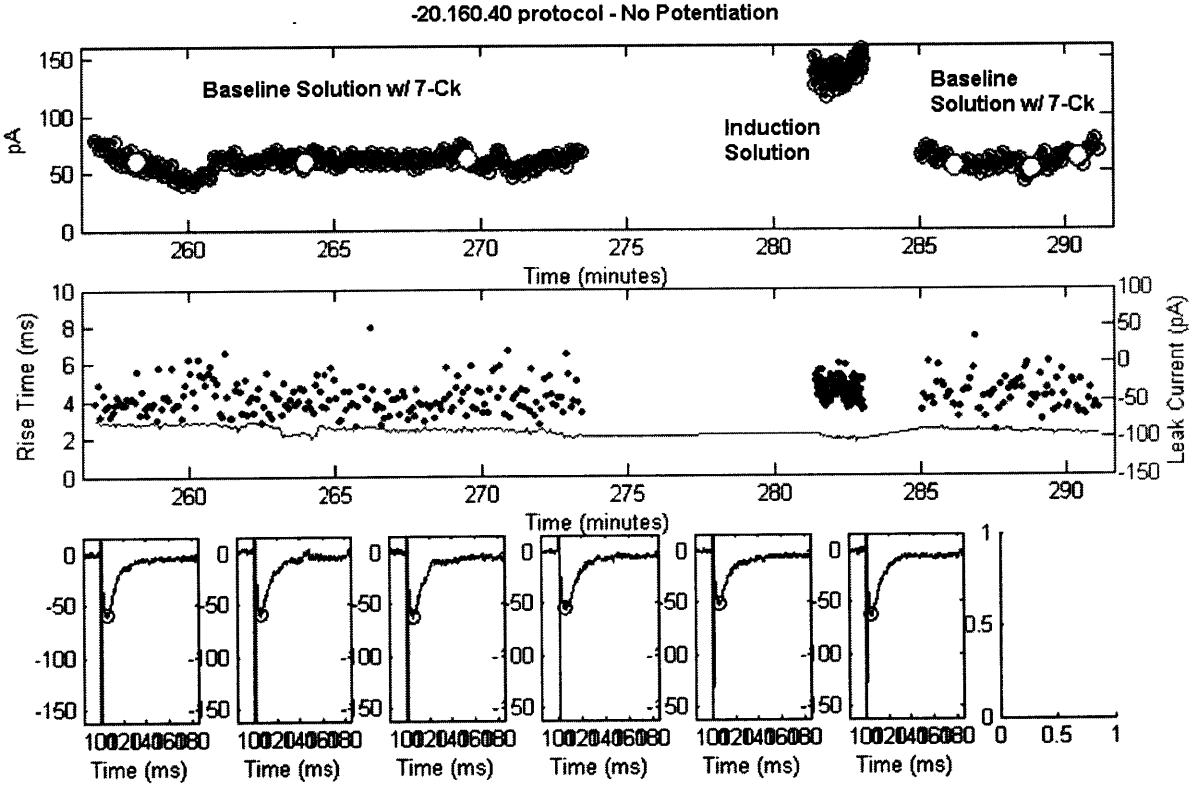

Figure 14: -30.160.1 induction protocol (-30 mV depolarization for the duration of 160 ms with 1Hz stimulation frequency) does not generate potentiation.

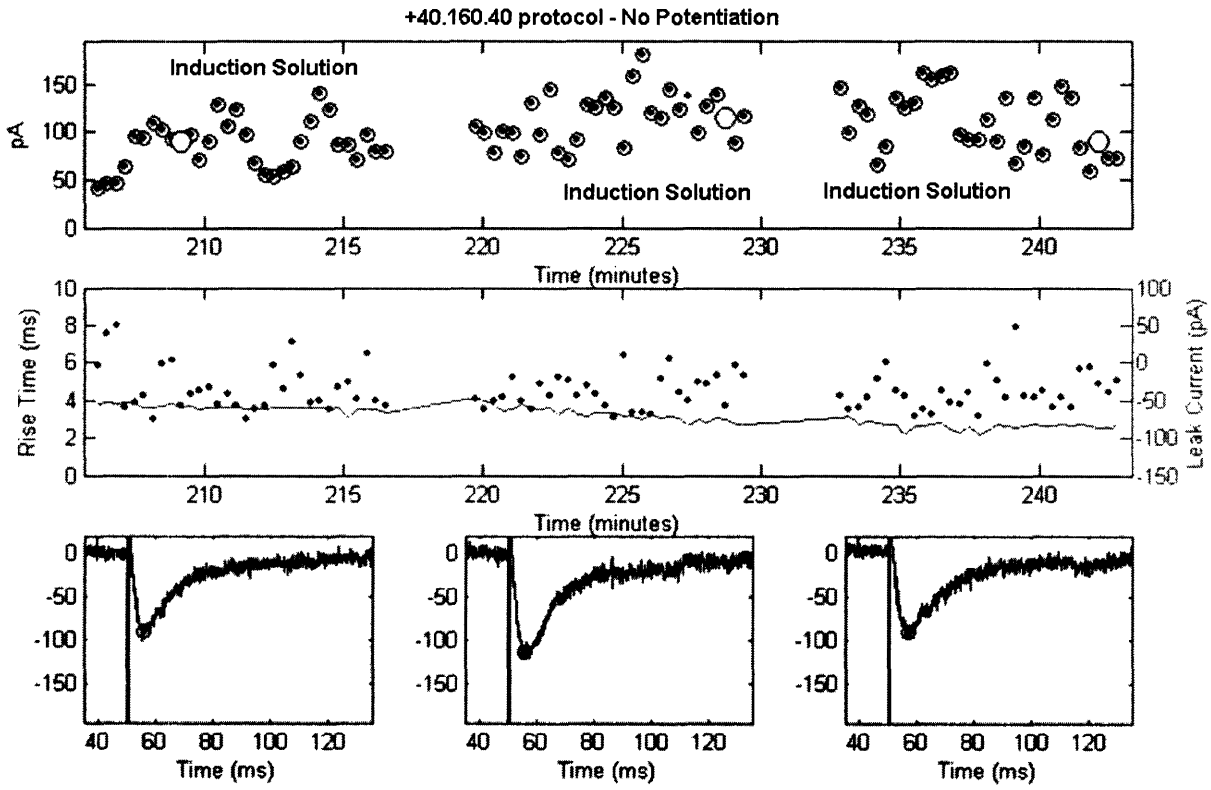

Figure 15: +30.160.1 induction protocol (+30 mV depolarization for the duration of 160 ms with 1Hz stimulation frequency) does not generate potentiation.

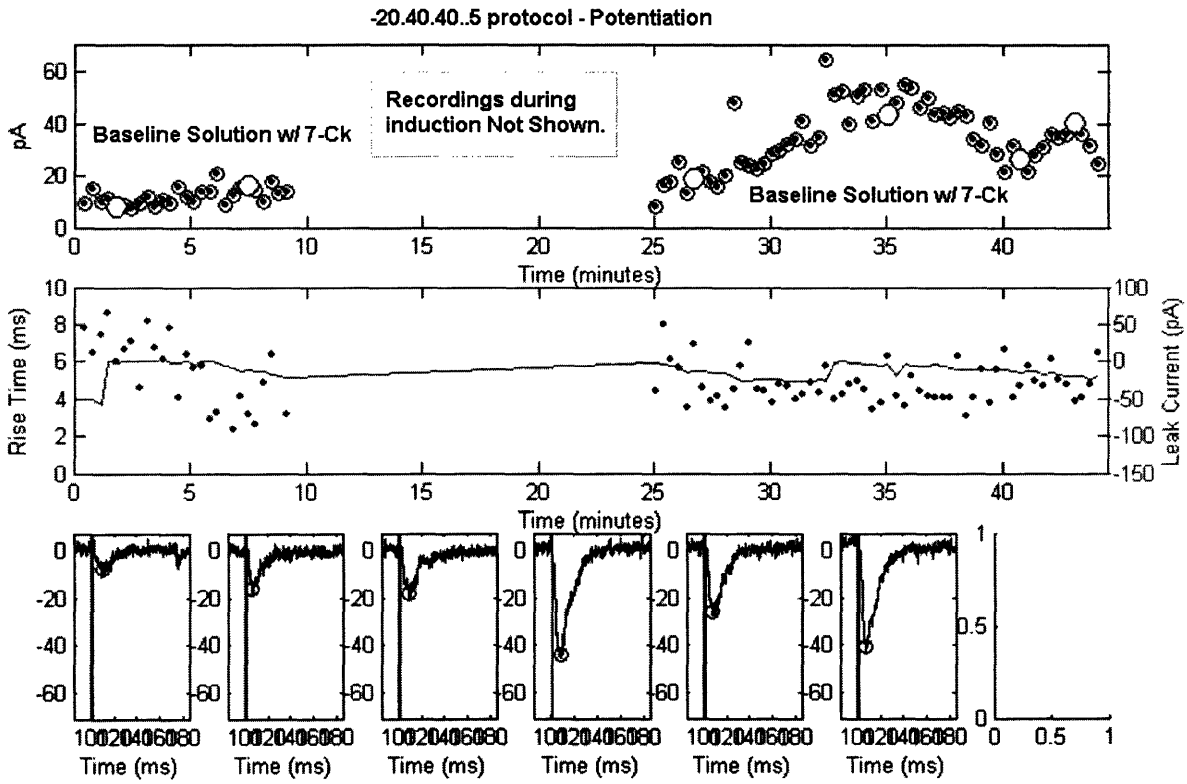

Figure 16: -30.40.0.2 induction protocol (-30 mV depolarization for the duration of 40 ms with 0.2Hz stimulation frequency) generates massive potentiation most of time.

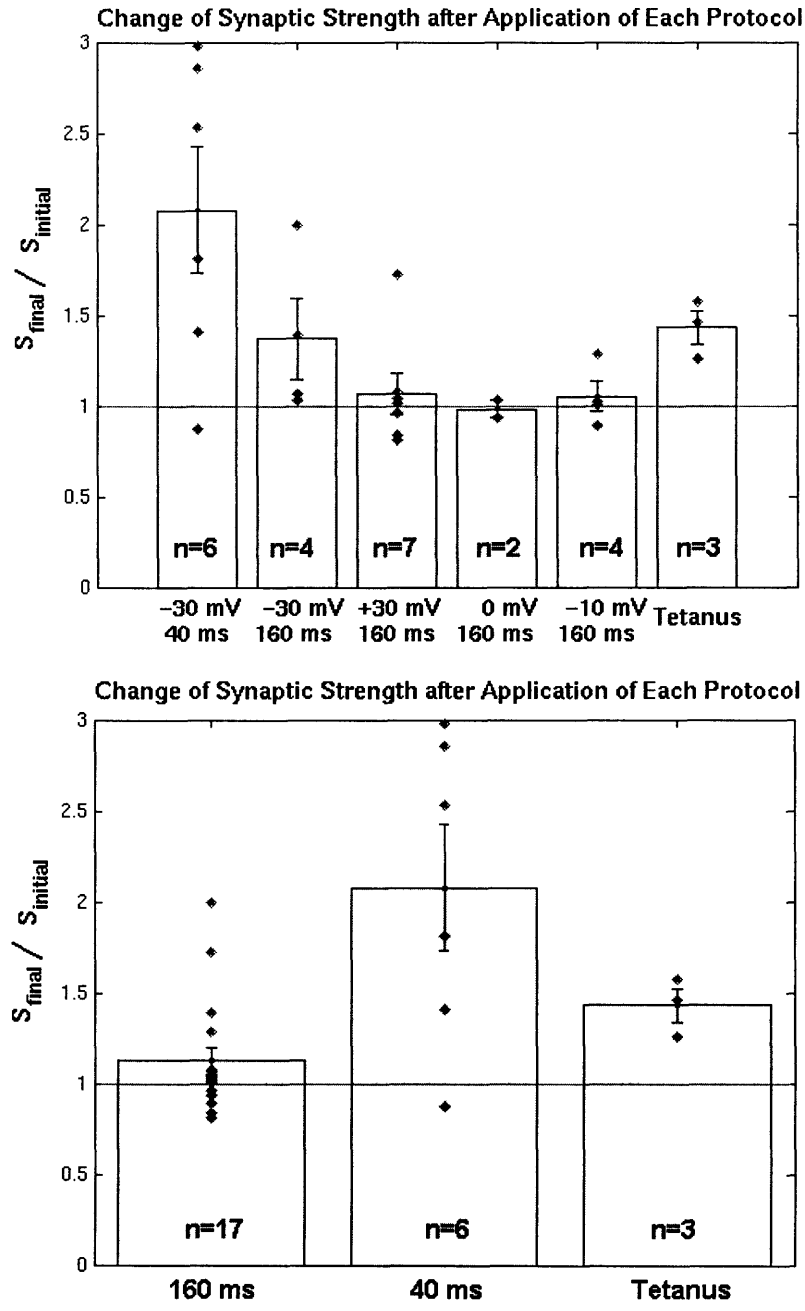

Figure 17: Summary of potentiation generation by several induction protocols. On average, $-10.160.0.2$ generated $4.9 \pm 8.3\%$ increase, $-30.160.1$ generated $37 \pm 22\%$ increase, $-30.40.0.2$ generated $108 \pm 35\%$ increase, $+30.160.1$ generated $6.4 \pm 12\%$ increase, and tetanus evoked $43 \pm 9.1\%$ increase as shown on the upper figure. In general, 160 ms, 1Hz protocols did not generate potentiation regardless of their depolarization voltage.

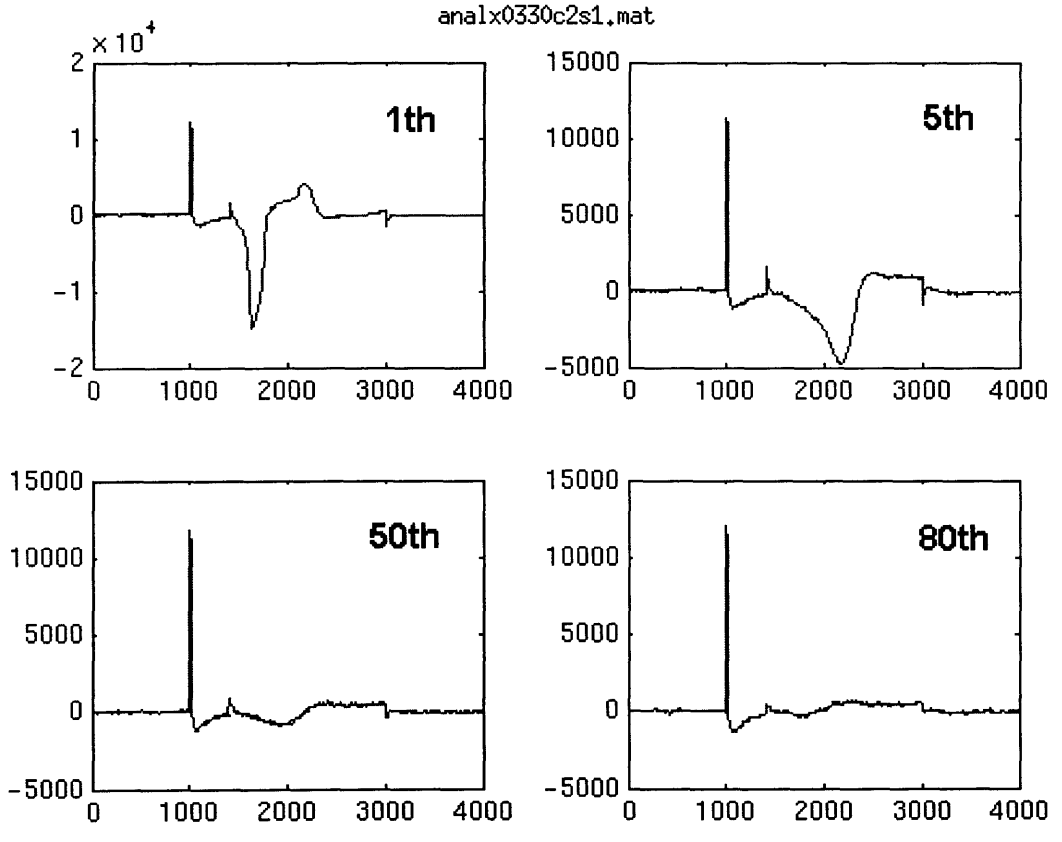

Figure 18: Desensitization of NMDA receptors under -30.160.1 induction protocol. Once large inward current diminishes in $\approx$ 10 stimulation cycles.

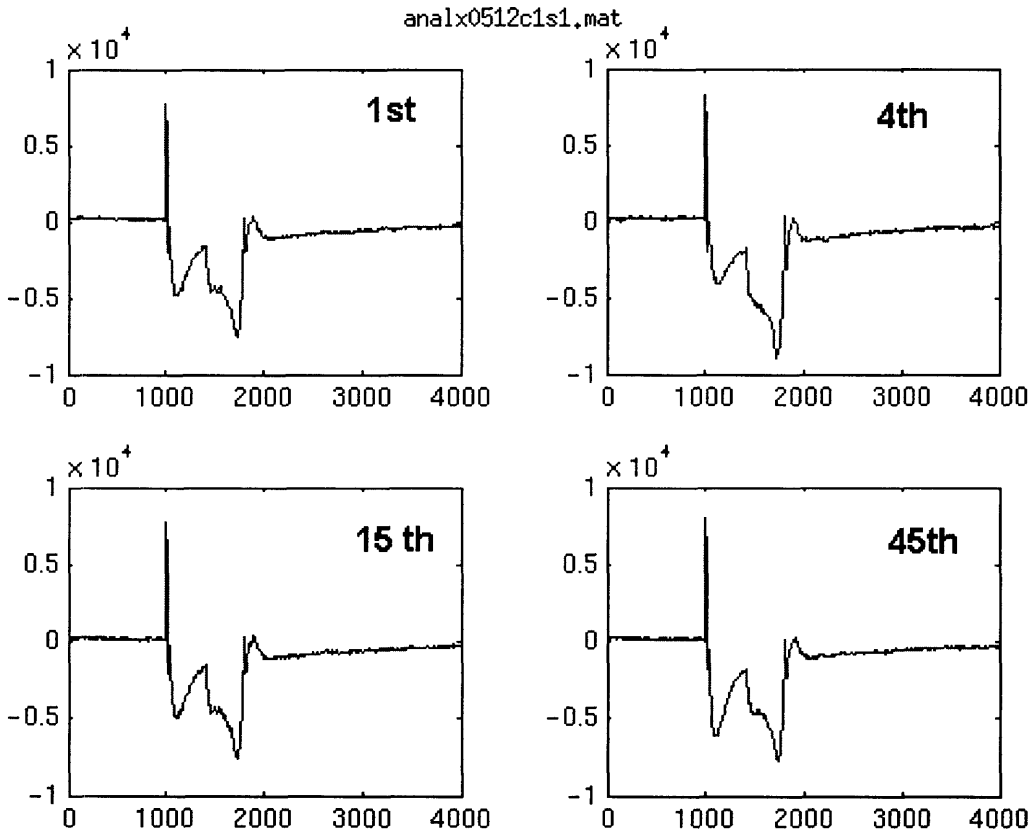

Figure 19: No desensitization effect of NMDAR responses under -30.40.0.2 induction protocol. The NMDAR responses are stable throughout the stimulation protocol.

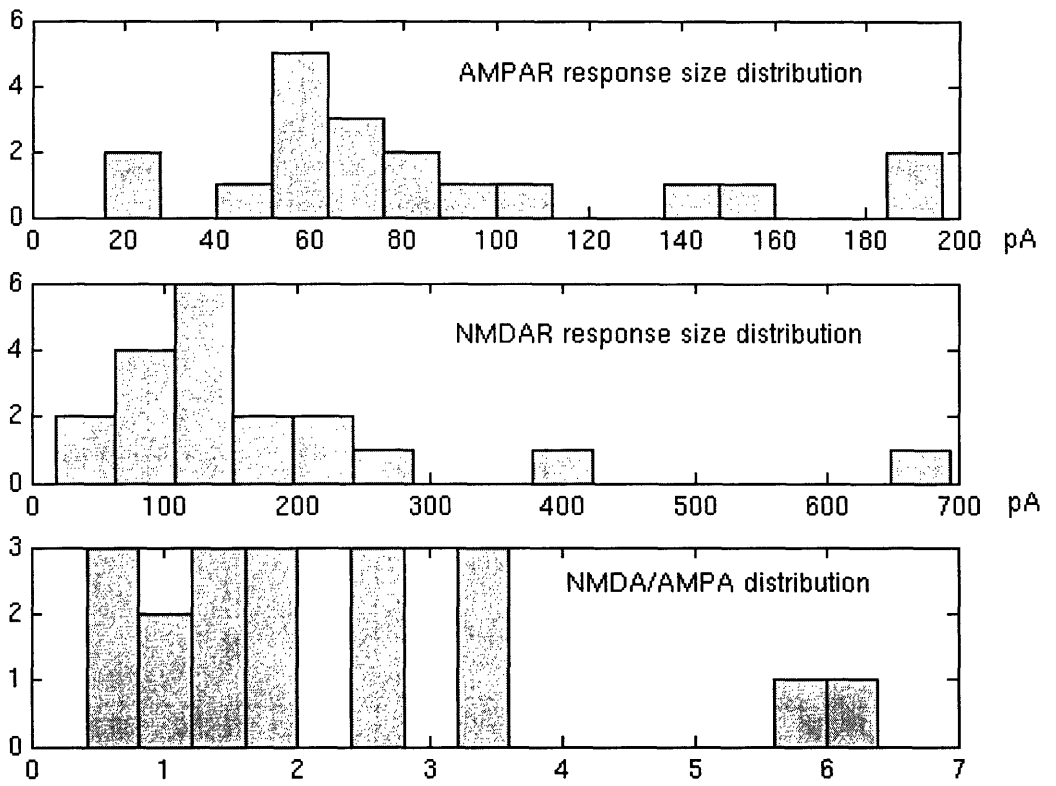

Figure 20: Distribution of AMPAR and NMDAR response sizes and their ratio.

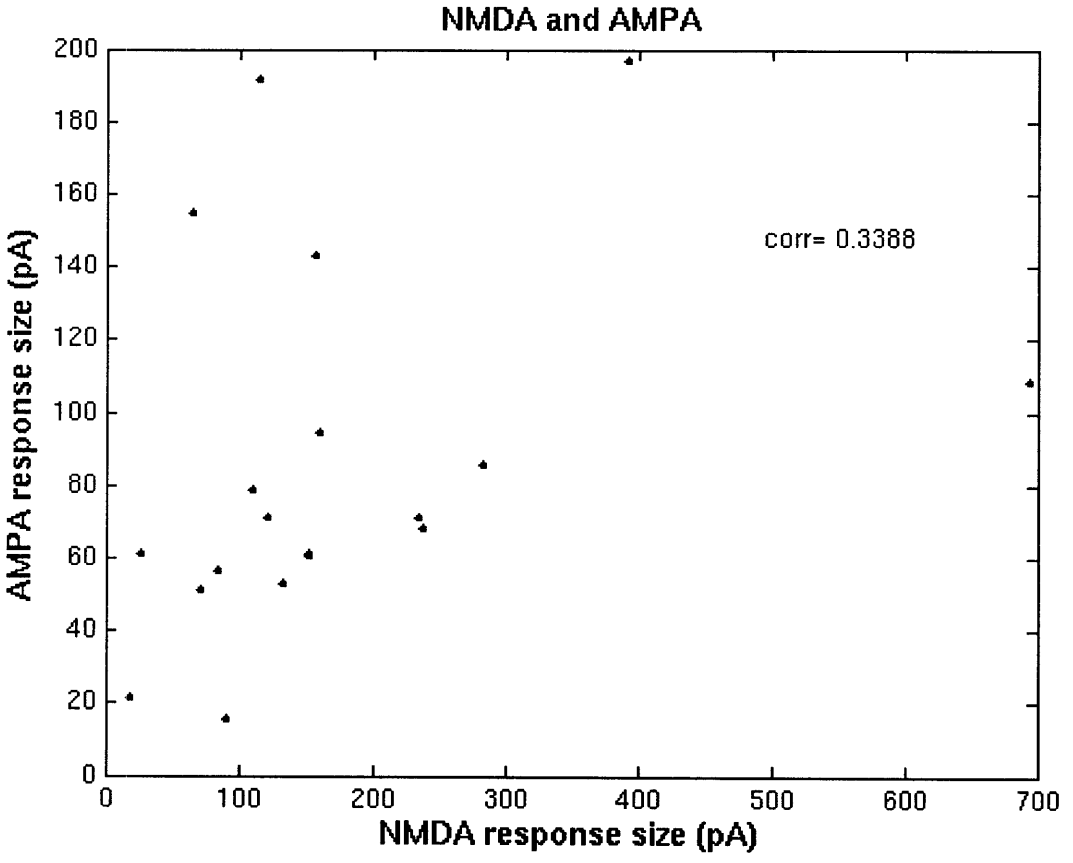

Figure 21: The NMDAR response size is not correlated with AMPAR response size.

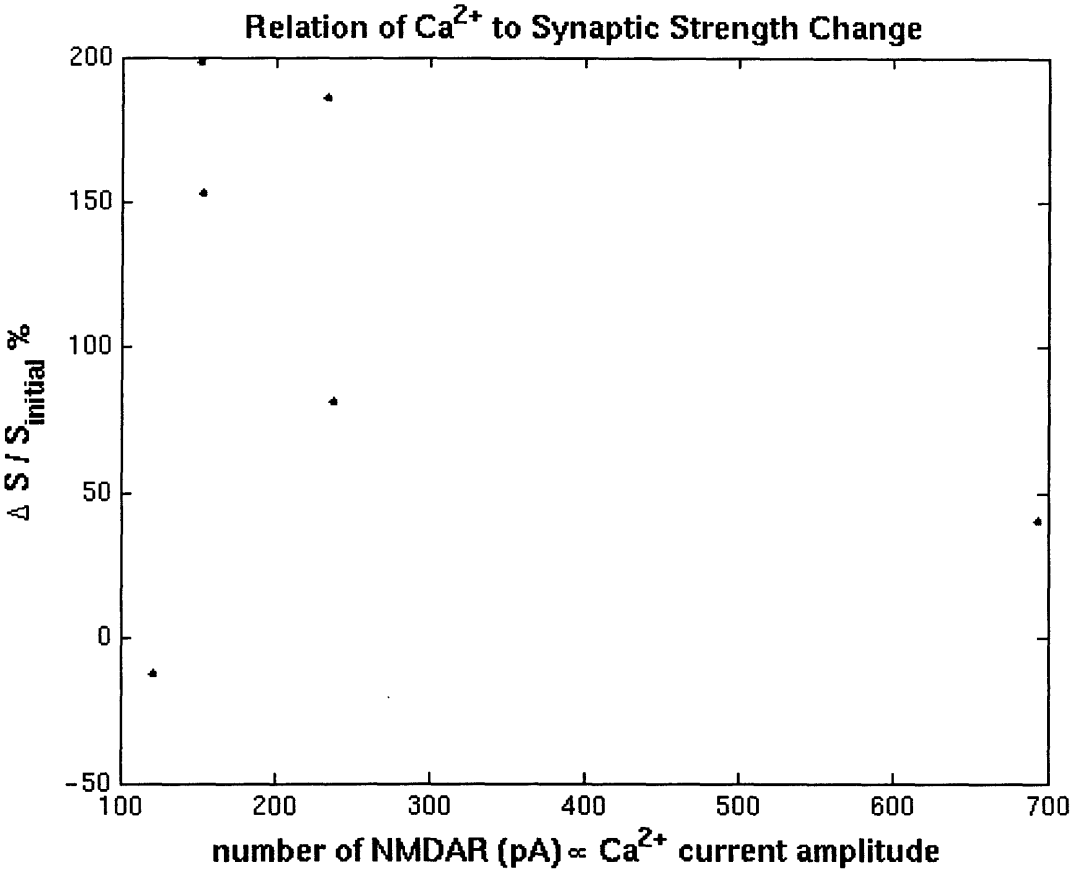

Figure 22: The amount of synaptic strength change is positively correlated with Ca^{2+} influx below 300pA. At large influx, potentiation level is low.

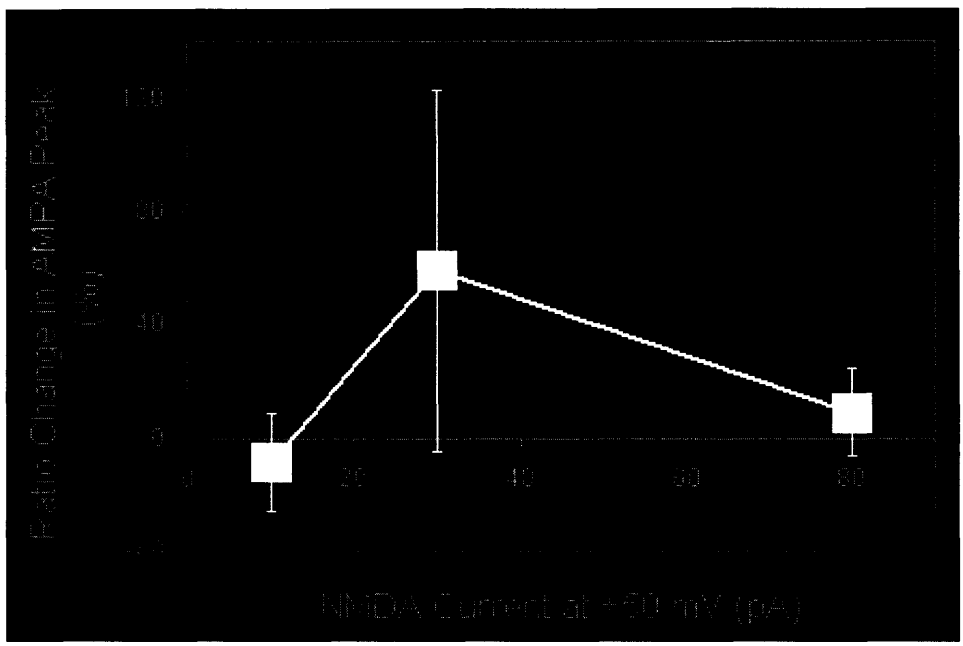

Figure 23: The previous result [24] also displays initially increasing then decreasing dependence of synaptic strength modification on Ca^{2+}.

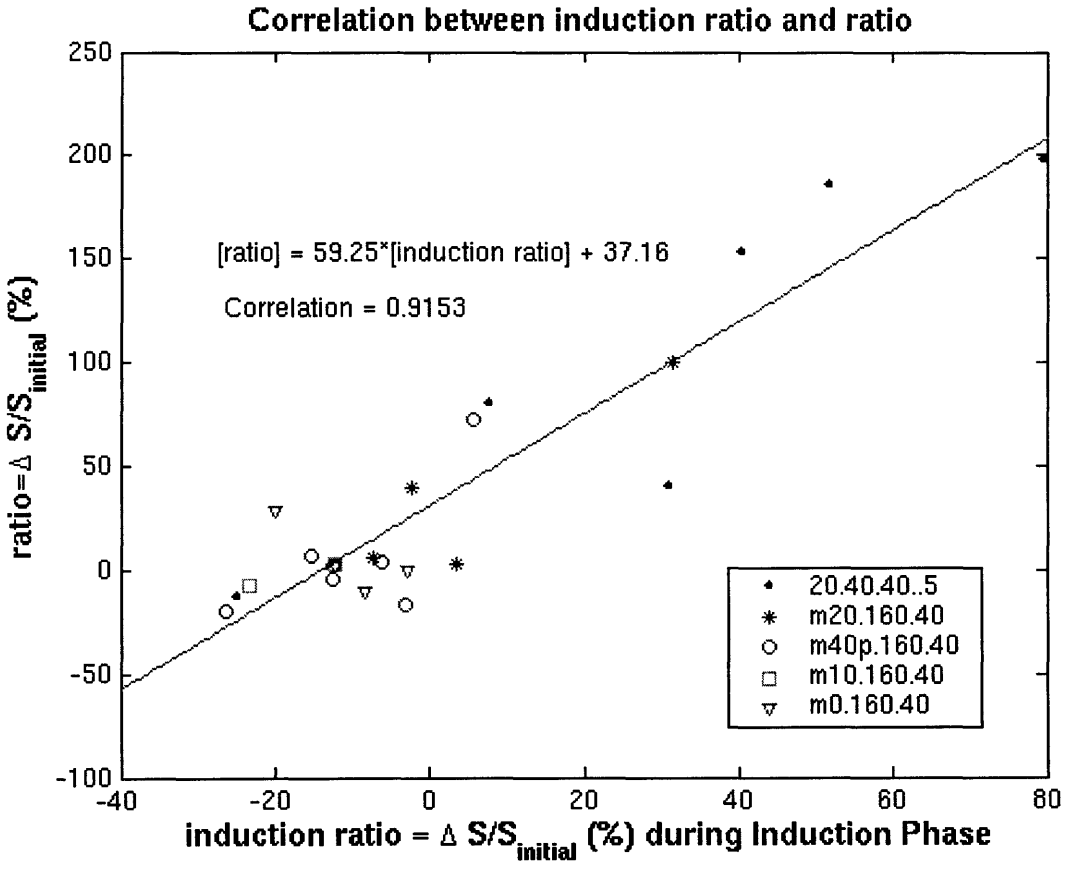

Figure 24: There is a large positive correlation between overall synaptic strength change ($\Delta S/S_{\text{initial}}$) and the short-term-plasticity during induction protocol (induction ratio) regardless of the induction protocols.